6738–6753 *Nucleic Acids Research, 2023, Vol. 51, No. 13* *Published online 2 June 2023*
https://doi.org/10.1093/nar/gkad481

Mechanistic insight into AP-endonuclease 1 cleavage of abasic sites at stalled replication fork mimics

Nicole M. Hoitsma[1], Jessica Norris[2], Thu H. Khoang[1], Vikas Kaushik[3], Rahul Chadda[3], Edwin Antony[3], Mark Hedglin[2] and Bret D. Freudenthal[1,*]

[1]Department of Biochemistry and Molecular Biology, University of Kansas Medical Center, Kansas City, KS 66160, USA, [2]Department of Chemistry, The Pennsylvania State University, University Park, PA 16802, USA and [3]Department of Biochemistry and Molecular Biology, Saint Louis University School of Medicine, St. Louis, MO 63104, USA

Received November 07, 2022; Revised May 13, 2023; Editorial Decision May 15, 2023; Accepted May 31, 2023

ABSTRACT

Many types of damage, including abasic sites, block replicative DNA polymerases causing replication fork uncoupling and generating ssDNA. AP-Endonuclease 1 (APE1) has been shown to cleave abasic sites in ssDNA. Importantly, APE1 cleavage of ssDNA at a replication fork has significant biological implications by generating double strand breaks that could collapse the replication fork. Despite this, the molecular basis and efficiency of APE1 processing abasic sites at replication forks remain elusive. Here, we investigate APE1 cleavage of abasic substrates that mimic APE1 interactions at stalled replication forks or gaps. We determine that APE1 has robust activity on these substrates, like dsDNA, and report rates for cleavage and product release. X-ray structures visualize the APE1 active site, highlighting an analogous mechanism is used to process ssDNA substrates as canonical APE1 activity on dsDNA. However, mutational analysis reveals R177 to be uniquely critical for the APE1 ssDNA cleavage mechanism. Additionally, we investigate the interplay between APE1 and Replication Protein A (RPA), the major ssDNA-binding protein at replication forks, revealing that APE1 can cleave an abasic site while RPA is still bound to the DNA. Together, this work provides molecular level insights into abasic ssDNA processing by APE1, including the presence of RPA.

GRAPHICAL ABSTRACT

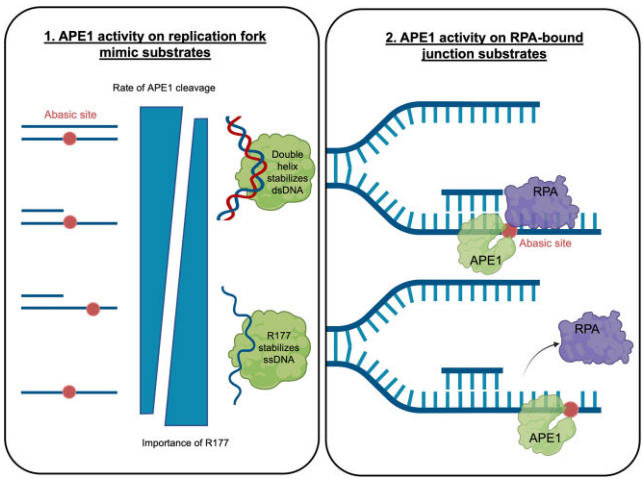

INTRODUCTION

Abasic sites are one of the most frequent types of DNA damage, with an estimated occurrence of ∼10 000–20 000 per human cell per day. These non-coding lesions are generated through spontaneous depurination or enzymatic processing by DNA glycosylases, which remove the nitrogenous base and leave behind a baseless sugar moiety (1–4). If not repaired, abasic sites act as a block to replicative DNA polymerases during DNA replication. In either leading or lagging stand replication, the DNA polymerase will pause when it encounters an abasic site, ultimately stalling at a 3′ dsDNA–ssDNA primer-template junction (PTJ) (5–9). However, the DNA helicase will continue forward, uncoupling replication fork progression from the polymerase and generating stretches of single-stranded DNA (ssDNA), which are coated by the ssDNA binding protein complex, Replication Protein A (RPA) (10–12). As these stretches of ssDNA are more vulnerable to chemical attack and spontaneous base loss than dsDNA, additional abasic sites can

*To whom correspondence should be addressed. Tel: +1 913 588 5560; Email: bfreudenthal@kumc.edu

form at sites of stalled DNA replication (3,13). Furthermore, additional abasic sites accumulate on ssDNA through APOBEC enzymes deaminating cytosines in ssDNA and the subsequent processing by uracil N-glycosylase (UNG) (3,14–19). Despite this, it remains unclear how abasic sites at replication forks are targeted to distinct bypass/repair pathways. Processing is hypothesized to occur via a number of pathways (Supplementary Figure S1) that include, but are not limited to: (i) the abasic site can be cleaved by the nuclease Apurinic/Apyrimidinic Endonuclease 1 (APE1) generating a double strand DNA break, (ii) the abasic site can be covalently attached to the HMCES protein generating a DNA protein crosslink, and/or (iii) the abasic site can be bypassed by translesion DNA polymerases generating mutations due to the lack of coding potential (19–26).

As an essential enzyme in the base excision repair pathway, APE1 has a well characterized cleavage activity processing abasic sites in double stranded DNA (dsDNA) (27,28). However, APE1 also cleaves abasic sites in a variety of other biologically relevant substrates, including single stranded DNA (ssDNA), making any abasic site near the replication fork a potential cleavage site for APE1 (29,30). APE1 cleavage of ssDNA has significant biological implications when DNA replication is stalled because it generates a double stranded break, which could collapse the replication fork. Despite the biological implications of APE1 cleavage at the replication fork, the molecular basis for APE1 recognizing and processing abasic sites in substrates mimicking stalled replication remains unknown. This is particularly important given the abundant concentration of cellular APE1, approximately 0.35 to 7 $\times$ 10^6 molecules per cell (31), and data showing physical association of APE1 with components of the replication machinery (32–34). Furthermore, evidence that there is an APE1-dependent degradation of stalled replication forks in response to DNA damage demonstrates the significance of APE1 in replication fork stability (35).

Here, we study APE1 cleavage activity at abasic DNA substrates that mimic potential APE1 interactions at a stalled replication fork and/or gap using a combination of kinetic and structural approaches. We determine that APE1 is active on these substrates, reporting pre-steady-state kinetic rates for both cleavage and product release. X-ray crystallography reveals molecular details of the APE1 active site during catalysis, including active site contacts and residues that mediate cleavage of abasic sites in ssDNA, highlighting that APE1 uses a similar mechanism to process ssDNA and dsDNA substrates. Through mutational and kinetic analysis, we determine residue R177 to be critical for the APE1 ssDNA cleavage mechanism. Furthermore, we investigated the interplay between APE1 and RPA on these substrates. Data reveals that APE1 is able to catalyze cleavage of the phosphodiester backbone with RPA bound to the DNA substrate. Together these data provide insight into the complex role of APE1 at stalled replication forks and gaps, including its activity in the presence of RPA.

MATERIALS AND METHODS

DNA sequences

DNA oligonucleotides were synthesized by Integrated DNA Technologies (Coralville, IA) and concentrations were determined from the absorbance at 260 nm using the calculated extinction coefficients. The concentrations of Cy3-labeled DNAs were determined from the extinction coefficient at 550 nm for Cy3 (ε_{550} = 136 000 M^{-1} cm^{-1}). For annealing two single strand DNAs (as depicted in Supplementary Figure S2), the primer and corresponding complementary template strands were mixed in equimolar amounts in 1X Annealing Buffer (10 mM Tris–HCl, pH 8.0, 100 mM NaCl, 1 mM EDTA), heated to 95°C for 5 min, and allowed to slowly cool to room temperature at a rate of 1°C min^{-1} to 4°C. The ssDNA substrate sequence used for kinetics and binding assays was: 5′-*GCT-GAT-GCG-CXC-GAC-GGA-TCC-3′, where * denotes a fluorescein and X denotes abasic site analog, THF. For crystallization of the APE1:ssDNA complex the following ssDNA sequence was used: 5′-ATCCGAXCGATGC-3′.

Protein expression and purification

Several different human APE1 proteins were used in this study: full length (FL) wild-type (WT) APE1 and full length APE1 R177A for activity assays, full length catalytically dead APE1 D210N/E96Q ($APE1_{Dead}$) for binding and FRET assays, and truncated (lacking the N-terminal 42 amino acids) APE1 C138A (ΔAPE1) for crystallography (Supplementary Figure S3). All of these APE1 proteins were expressed and purified as previously described (36). Mutagenesis was done via Quick-change II site-directed mutagenesis (Agilent) and mutations were confirmed via Sanger sequencing. Plasmids, pet28a codon optimized, were overexpressed in BL21(DE3) plysS *E. coli* cells (Invitrogen). Expression was induced with isopropyl β-D-1-thiogalactopyranoside before cells were harvested and lysed via sonication. APE1 protein was purified from the cell lysate using column chromatography. The resins for this purification include heparin, cation exchange, and gel filtration resins on an ATKA-Pure FPLC. Purified protein was monitored throughout the purification process via SDS-PAGE. After column chromatography, pure fractions were pooled, and final concentration was determined via absorbance at 280 nm. Concentrated APE1 protein was stored at -80°C in a buffer of 50 mM HEPES (pH 7.4) and 150 mM NaCl.

Human RPA was obtained as previously described (37). The concentration of active RPA was determined via a FRET-based activity assay as described previously (38). Human RPA containing a Cy5 label at position 107 of the RPA32/RPA2 subunit (Cy5-OBD-RPA) was obtained essentially as described for *S. cerevisiae* RPA (39,40). Residue 107 of the RPA32 subunit resides in the oligonucleotide-binding folds (OB-fold) D of the human RPA heterotrimeric complex (Supplementary Figure S3).

APE1 activity assays

Reactions were initiated by mixing APE1 enzyme with DNA substrate in reaction buffer containing a final concentration of 50 mM HEPES, pH 7.5, 100 mM KCl, 5 mM $MgCl_2$ and 0.1 mg/ml bovine serum albumin (BSA) at 37°C. Different APE1 and DNA final concentrations were used dependent upon the kinetic regime for each assay. For multiple turnover kinetics, DNA is in excess of APE1 at final

concentrations of 100 and 30 nM, respectively. For single turnover kinetics, APE1 is in excess of DNA at final concentrations of 500 and 50 nM, respectively. After mixing, the reactions were allowed to progress for a pre-determined amount of time before being quenched with EDTA. Multiple and single turnover pre-steady-state kinetics were completed at very rapid timepoints, and thus were carried out using a rapid quench flow system (KinTek) which allows rapid mixing as fast as 0.002 s. Temperature is controlled with a circulating water bath in the instrument allowing experiments to be carried out at 37°C. Longer time points used for the product formation assay (1 and 10 min) allowed reactions to be completed in a benchtop heat block at 37°C. Quenched reactions were mixed with loading dye (100 mM EDTA, 80% deionized formamide, 0.25 mg/ml bromophenol blue and 0.25 mg/ml xylene cyanol) and incubated at 95°C for 6 min. Reactions products were separated via denaturing polyacrylamide gel electrophoresis. DNA oligonucleotides used in this assay (described above) contain a 5′ fluorescein label (6-FAM) allowing substrate and product bands to be visualized with a Typhoon imager in fluorescence mode. Analysis of the imaged gel is completed by quantifying the bands using ImageQuant software, plotted and fit using Prism. To quantitatively determine rate values, multiple turnover time courses were fit to the following equation: product $= A(1 - e^{-k_{obs}t}) + v_{ss}t$, where A represents the amplitude of the rising exponential which corresponds to the fraction of actively bound enzyme, and k_{obs} is the first order rate constant. The steady-state rate constant (k_{ss}) is the steady-state velocity (v_{ss})/A. Single turnover experiments for wild-type APE1 are fit to single exponential equation: product $= A(1 - e^{-k_{obs}t})$. Single turnover experiments for R177A mutant are fit to double exponential equation: product $= A(1 - e^{-k_1 t}) + B(1 - e^{-k_2 t})$, as seen previously (41). Each time point in the curves for both single and multiple turnover kinetics represents an average of at least three independent experiments ± standard error as determined using Prism analysis software.

Electrophoretic mobility shift assay

Full length catalytically dead APE1 D210N/E96Q ($APE1_{Dead}$) was utilized in binding experiments to prevent cleavage, which would convolute binding analysis. In these experiments, annealed or single stranded DNA substrates (5 nM) were mixed with varying amount of APE1 (0–2000 nM) in reaction buffer containing a final concentration of 50 mM Tris (pH 8), 1 mM EDTA, 0.2 mg/ml BSA, 1 mM DTT and 5% v/v sucrose (for purposes of gel loading). Samples are equilibrated at room temperature for 20 minutes before separation on a 10% native 59:1 polyacrylamide gel run at 120 V with 0.2× TBE running buffer. DNA oligonucleotides used in this assay (described above) contain a 5′ fluorescein label (6-FAM) which allows free and bound DNA bands to be visualized using a Typhoon imager in fluorescence mode. Analysis is completed by quantifying the free DNA bands using ImageQuant software, plotted and fit using Prism to Equation (1):

$$\mathbf{AB} = \frac{(\mathbf{A_T} + \mathbf{B_T} + \mathrm{K_{D,app}}) - \sqrt{(\mathbf{A_T} + \mathbf{B_T} + \mathrm{K_{D,app}})^2 - 4(\mathbf{A_T B_T})}}{2} \quad (1)$$

where A_T and B_T represent the total concentration of APE1 and DNA, respectively, and AB is the concentration of APE1:DNA complex used to determine apparent affinity ($K_{D,app}$). Each data point represents an average of at least three independent experiments ± standard error as determined using Prism software.

X-ray crystallography

For crystallization of APE1:ssDNA product complex, the ssDNA oligo was mixed with ΔAPE1 C138A at a final concentration of 0.56 nM DNA and 10–12 mg/ml APE1. The truncation of N-terminal 42 amino acids and C138A mutation are commonly utilized to aid in APE1 crystallization (42,43). As this is a catalytically competent APE1 enzyme, product formation likely occurs during a 30-min incubation period at room temperature, prior to setting up crystallization trays. APE1:ssDNA product complex crystals were generated via sitting drop vapor diffusion using 2 ul protein/DNA mix combined with 2 ul reservoir solution (0.05 M KCl; 0.05M sodium cacodylate pH 6; 10% PEG 8000; 5 mM spermine; 5 mM L-argininamide dihydrochloride). Resultant crystals were transferred to a cryoprotectant solution containing reservoir solution supplemented with 20% ethylene glycol, flash frozen, and subjected to X-ray diffraction. The APE1:ssDNA product structure was collected at 100 K on a Rigaku MicroMax-007 HF rotating anode diffractometer system at a wavelength of 1.54 Å. This system utilizes a Dectris Pilatus3R 200K-A detector and HKL3000R software was used for processing and scaling the data after collection. Initial models were determined using molecular replacement in PHENIX with a modified version of a previously determined APE1:DNA complex structure (PDB: 5DFF). Refinement and model building were done with PHENIX and Coot, respectively, and figures were made using PyMol (Schrödinger LLC) (44,45).

Mass photometry

All measurements were carried out on TwoMP instrument (Refeyn Ltd.). Glass coverslips (No. 1.5H thickness, 24 × 50 mm, VWR) were cleaned by sonicating, first in isopropanol, and then in deionized water for 15 min, each. Afterwards, the coverslips were dried under a stream of filtered nitrogen. For each round of measurement, a clean coverslip was placed on the oil-immersion objective lens (Olympus PlanApo N, 1.42 NA, 60×), with a holey-silicone gasket (Refeyn Ltd) adhered on the top surface of the coverslip. All dilutions and measurements were performed at room temperature (23 ± 2°C) and, unless indicated otherwise, in 1× Mg^{2+}/Ca^{2+} buffer (20 mM HEPES, pH 7.5, 150 mM KCl, 5 mM $MgCl_2$, 5 mM $CaCl_2$) supplemented with 1 mM DTT and the ionic strength was adjusted to physiological (200 mM) by the addition of appropriate amounts of KCl. Samples of DNA alone, hRPA alone, or DNA-RPA mixtures were allowed to equilibrate for 5 min after which 1 μl of the respective sample was quickly diluted 15-fold onto the sample stage and video recording commenced and continued for 1 min. High contrast (light-scattering) events corresponding to single particle landings on the coverslip were identified and analyzed further. A known mass standard

(β-amylase, SIGMA A8781-1VL) was used to convert image contrast-signal into mass units. Histograms were plotted from all the data gathered during the 1 min video interval and non-linear least squares fit to single or mixture Gaussian functions (Equation 2) to extract relevant parameters and discern underlying populations.

$$f(x) = \sum a_n exp^{-\left(\frac{x-b_n}{c_n}\right)^2} \quad (2)$$

where a_n, b_n and c_n are the amplitude, mean and the standard deviation of the nth Gaussian component.

Ensemble FRET measurements

All experiments were performed at room temperature (23 ± 2°C) and, unless indicated otherwise, in 1× Mg^{2+}/Ca^{2+} buffer (20 mM HEPES, pH 7.5, 150 mM KCl, 5 mM $MgCl_2$, 5 mM $CaCl_2$) supplemented with 1 mM DTT and the ionic strength was adjusted to physiological (200 mM) by the addition of appropriate amounts of KCl. All experiments were performed in a Horiba Scientific Duetta-Bio fluorescence/absorbance spectrometer. Solutions are excited at 514 nm and the fluorescence emission intensities (I) are simultaneously monitored at 563 nm (I_{563}, Cy3 FRET donor fluorescence emission maximum) and 665 nm (I_{665}, Cy5 FRET acceptor fluorescence emission maximum) over time, recording I every 0.17 s. For each time point, E_{FRET} is calculated where $E_{FRET} = \frac{I_{665}}{I_{665}+I_{563}}$. For all FRET experiments, excitation and emission slit widths are 20 nm. For RPA/$APE1_{Dead}$ titration exchange experiments, a solution containing a 3′ Cy3-labeled PTJ DNA (25 nM) is pre-saturated with Cy5-RPA (absolute concentration indicated in respective figure legend) and the resultant mixture is then titrated with increasing amounts of $APE1_{Dead}$ and the E_{FRET} values at each protein amount is calculated as follows. At each protein amount, E_{FRET} values are recorded every 0.17 s until the FRET maintains a constant value for at least 1 minute and the data points within this stable region are averaged to obtain the final E_{FRET} value. To determine the predicted E_{FRET} value for Cy5-RPA remaining completely disengaged from a 3′ Cy3-labeled PTJ DNA, the fluorescence emission intensities (I_{665} and I_{563}) for Cy5-RPA alone and the respective Cy3-PTJ DNA alone are each recorded over time, and E_{FRET} is calculated for each time point as follows; $E_{FRET} = \frac{(I_{665}^{RPA}+I_{665}^{DNA})}{(I_{665}^{RPA}+I_{665}^{DNA})+(I_{563}^{RPA}+I_{563}^{DNA})}$. For RPA/DNA titration exchange experiments, a solution containing a Cy3-labeled PTJ DNA substrate (25 nM, either Cy3-PTJ or Cy3-Rec-PTJ, Supplementary Figure S2) is pre-saturated with Cy5-RPA (≤75 nM absolute protein complex) and the resultant mixture is then titrated with increasing amounts of either an unlabeled PTJ DNA (either PTJ or Rec-PTJ, Supplementary Figure S2) or full length catalytically dead APE1 D210N/E96Q ($APE1_{Dead}$) and the E_{FRET} values at each concentration of titrant is calculated as described above. The predicted E_{FRET} value for Cy5-RPA remaining completely disengaged from the respective Cy3-PTJ DNA is determined as described above. For experiments in which unlabeled PTJ DNA is the titrant, data is normalized to a range defined by the E_{FRET} observed in the absence of unlabeled competitor DNA (i.e. Y-Max) and the predicted E_{FRET} value for Cy5-RPA remaining completely disengaged from the Cy3-PTJ DNA (i.e. Y-Min). It should be noted that in all assays where Cy5-RPA is utilized, the absolute concentrations of the added RPA complex are indicated in the respective figure legends. In all assays utilizing Cy5-RPA, the absolute concentration of RPA is saturating and the ratio of absolute RPA complex:DNA does not exceed 3:1. Previous studies of human RPA suggest that binding of multiple RPA complexes to a single strand DNA (ssDNA) sequence ∼30 nt in length is not significantly observed at moderate RPA:DNA ratios (i.e. ≤10:1) (46–48). Indeed, in the current study, only a single RPA complex engages a free 35-mer ssDNA sequence (Supplementary Figure S4) at a 4:1 RPA:DNA ratio. Furthermore, at a 3:1 ratio of RPA:DNA, DNA:RPA complexes with 2 RPA per DNA accounted for only ∼10% of the observed RPA interactions on a PTJ DNA substrate with a 30-mer ssDNA sequence (Supplementary Figure S5). When the ssDNA sequence of a PTJ DNA substrate is extended to 80 nucleotides, DNA:RPA complexes with 2 RPA per DNA accounted for only ∼20% of the observed RPA interactions at a 3:1 ratio of RPA:DNA (Supplementary Figure S5).

APE1 activity in the presence of RPA

These experimental conditions were designed to mimic the conditions of the FRET assay. All experiments were performed at room temperature in 1× Mg^{2+}/Ca^{2+} buffer (20 mM HEPES, pH 7.5, 150 mM KCl, 5 mM $MgCl_2$, 5 mM $CaCl_2$) supplemented with 1 mM DTT and the ionic strength was adjusted to physiological (200 mM) by the addition of appropriate amounts of KCl. A solution containing either the PTJ or Rec-PTJ DNA (100 nM) is pre-saturated with RPA protein (200 nM). Reactions were initiated by mixing RPA-saturated DNA substrate with APE1 at varying concentrations (100, 500 and 1000 nM). After mixing, the reactions were allowed to progress for a predetermined amount of time before being quenched with EDTA. Quenched reactions were mixed with loading dye (100 mM EDTA, 80% deionized formamide, 0.25 mg/ml bromophenol blue and 0.25 mg/ml xylene cyanol) and incubated at 95°C for 6 min. Reactions products were separated via denaturing polyacrylamide gel electrophoresis. DNA oligonucleotides used in this assay were the same as those used for kinetic assays and thus contain a 5′ fluorescein label (6-FAM) allowing substrate and product bands to be visualized with a Typhoon imager in fluorescence mode. Analysis of the imaged gel is completed by quantifying the bands using ImageQuant software and graphed with Prism. Each bar represents an average of at least three independent experiments ± standard error as determined using Prism analysis software.

RESULTS

Quantification of APE1 kinetic rates on PTJ and ssDNA substrates

To study APE1 cleavage activity at stalled replication forks, we constructed three abasic DNA substrates that mimic various regions of a stalled replication fork or gap. Specifically, the substrates each contain a single abasic site ana-

log (tetrahydrofuran, THF) and were designed to represent varying degrees of interaction with a 3′ dsDNA–ssDNA primer-template junction (PTJ) (Figure 1A). Based on a structure of APE1 with duplex DNA (PDB 5DFI), the number of DNA nucleotides that interacts with APE1, termed its footprint, is about ten with APE1 centered at the abasic site (43,49). Utilizing this information, we designed the PTJ substrate to contain an abasic site directly next to the double stranded 3′ end, requiring APE1 to interact with the double stranded junction (Figure 1B). The second substrate, a recessed PTJ substrate (Rec-PTJ), places the abasic site 7 nucleotides away from the double stranded 3′ end. In this case, the APE1 footprint is only contacting ssDNA, but is near the double stranded junction. Finally, we also designed a ssDNA substrate lacking any adjacent dsDNA. Importantly, these substrates mimic common cellular situations. The PTJ substrate represents a DNA polymerase synthesizing right up to and stalling at the abasic site, the Rec-PTJ represents an abasic site near a primer template junction (such as within a post-replicative gap), and the ssDNA substrate represents an abasic site within a stretch of ssDNA upon replication fork uncoupling (Figure 1).

To quantitatively analyze the rate of APE1 cleavage activity, we performed pre-steady-state enzyme kinetics for this set of DNA substrates. Under a multiple turnover kinetic regime (in which the concentration of DNA (100 nM) was in excess of APE1 (30 nM)), the reaction produced a biphasic time course of product formation, consistent with what has been previously reported for APE1 endonuclease activity (Figure 2A and B) (41). This biphasic kinetic behavior is characterized by an initial burst phase corresponding to the first enzymatic turnover and the rate of DNA cleavage (k_{obs}), and is followed by a rate-limiting steady-state phase, presumably corresponding to the rate of product release (k_{ss}) (41). For the PTJ substrate, the k_{obs} and k_{ss} were determined to be 10 ± 1 and 2.7 ± 0.21 s^{-1}, respectively (Table 1). Compared to rates determined for APE1 on the canonical dsDNA substrate, this represents a 12.9-fold decrease in catalysis and a 1.6-fold increase in product release for the PTJ substrate. For the recessed PTJ substrate, which has the abasic site further removed from the double stranded junction, k_{obs} was 30 ± 4 s^{-1} and k_{ss} was 5.9 ± 0.32 s^{-1}, representing a 4.3-fold decrease in catalysis and 3.5-fold increase in product release (Table 1). For both PTJ substrates, the k_{obs} is <10-fold greater than the k_{ss} value, which makes accurate determination of k_{obs} difficult because the two phases are not easily differentiated during fitting.

To confirm the measured k_{obs} for both PTJ substrates, we performed additional single-turnover kinetic measurements. Consistent with the multiple-turnover measurements, the single turnover k_{obs} for the PTJ and Rec-PTJ substrates were determined to be 13.6 ± 0.4 and 25.7 ± 1.6 s^{-1}, respectively (Supplementary Figure S6). These results suggest that APE1 efficiently processes abasic sites at and near a primer template junction, with only a slight reduction in kinetic rate compared to dsDNA. Finally, for the ssDNA substrate, the k_{obs} was 2 ± 0.2 s^{-1} and k_{ss} was 0.15 ± 0.018 s^{-1}, representing a 64.5- and 11.3-fold decrease in activity compared to dsDNA, respectively (Table 1). This is the most significant reduction in cleavage we observed and suggests that the presence of some form of duplex DNA, as with the PTJ, is preferred for optimal APE1 activity. Together, these kinetic data indicate that APE1 processes PTJ and ssDNA substrates, though the associated catalytic rates are reduced compared to the exceedingly fast APE1 endonuclease activity on duplex DNA.

To determine the binding affinity of APE1 for these DNA substrates, we performed electrophoretic mobility shift essays (EMSAs) in the presence of EDTA to inhibit catalysis. Quantification of the EMSAs yielded $K_{d,app}$ values for the PTJ, Rec-PTJ, and ssDNA of 1.2 ± 0.1, 0.7 ± 0.05 and 22 ± 3 nM, respectively (Figure 2C and D). Both PTJ and Rec-PTJ substrates had a similar effect on APE1 binding compared to dsDNA ($K_{d,app} = 0.4 \pm 0.1$ nM), with a less than a 3-fold increase in their $K_{d,app}$. In contrast, the affinity for ssDNA was decreased 55-fold compared to dsDNA. Nonetheless, an apparent binding affinity of 22 ± 3 nM still represents a tight interaction of APE1 with ssDNA. Overall, these results demonstrate that APE1 binds to both the PTJ and the ssDNA substrates with a tight binding affinity.

Structural characterization of APE1 bound to a ssDNA substrate

To obtain structural insight into APE1 activity on ssDNA, we determined an X-ray crystal structure of APE1 bound to a ssDNA substrate (APE1:ssDNA). APE1:ssDNA crystals were generated using a 13-mer DNA oligonucleotide containing a centrally located abasic site analog. These crystals were generated in buffer conditions that included $MgCl_2$, which supports APE1 catalysis, resulting in a product complex. Due to these conditions, we have been unable to capture the substrate complex. The resulting APE1:ssDNA crystals diffracted to a resolution of 2.0 Å in space group P65 (Supplementary Table S1). The APE1:ssDNA complex structure represents a product complex, where APE1 catalysis has generated a nick in the DNA backbone. Importantly, as APE1 generated its product from substrate DNA, this signifies that APE1 is catalytically competent on the 13-mer ssDNA substrate. Moreover, as a result of APE1 cleavage, the downstream DNA sequence (5′ of the cleavage site) is not present in the structure of the APE1:ssDNA complex (Figure 3A). This is not surprising as APE1 has minimal interaction with DNA 5′ of the cleavage site.

The resulting APE1:ssDNA product complex reveals a well-formed APE1 active site, as seen previously for dsDNA structures (Figure 3B) (43,49,50). A single catalytic Mg^{2+} ion is directly coordinated by residue E96 and indirectly, through water-mediated interactions, by residues D70 and D308. Importantly, this Mg^{2+} is directly coordinated to the 5′-phosphate that is generated following cleavage. In the absence of the 3′-hydroxyl group (due to absence of the downstream DNA sequence in the crystal structure), an additional ordered water molecule coordinates the metal ion in the metal binding pocket. The non-bridging oxygens of the 5′-phosphate are coordinated by residues N212, D210, Y171 and H309, which stabilize the cleaved product complex.

Structural superimposition of the APE1:ssDNA product complex with the canonical APE1:dsDNA product complex (PDB: 5DFF) highlights the structural similarities between the two complexes. The overall structure of APE1 is

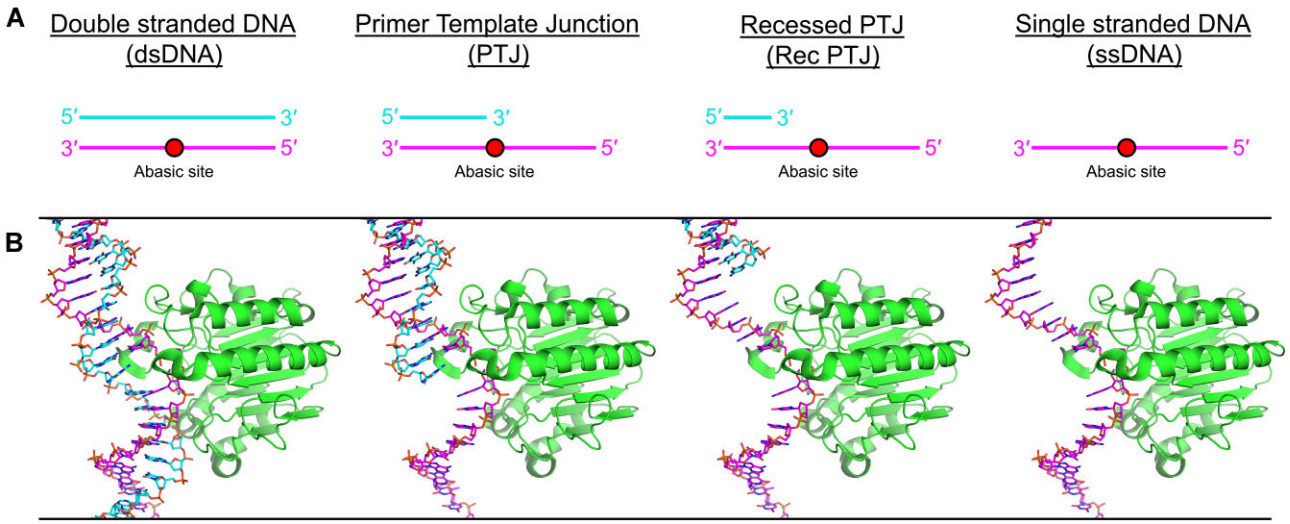

Figure 1. Primer-template junction and ssDNA substrate design. (**A**) Cartoon representation of DNA substrates (represented as a pink and cyan lines) with an abasic site (represented as a red circle). (**B**) Structural models of PDB 5DFI with APE1 (shown as green ribbon) and DNA (shown as pink and cyan sticks).

Table 1. Pre-steady-state multiple turnover kinetic parameters of wild-type APE1. Final concentrations of DNA at 100 nM, APE1 at 30 nM. Fold change is calculated from dsDNA values

Substrate	k_{obs} (s^{-1})	k_{obs} (fold change)	k_{ss} (s^{-1})	k_{ss} (fold change)
dsDNA	129 ± 24	–	1.7 ± 0.26	–
PTJ	10 ± 1	12.9 ± 2.6	2.7 ± 0.21	1.6 ± 0.3
Rec PTJ	30 ± 4	4.3 ± 0.9	5.9 ± 0.32	3.5 ± 0.6
ssDNA	2 ± 0.2	64.5 ± 12.9	0.15 ± 0.018	11.3 ± 0.4

very similar with an RMSD (Cα) of 0.307, with all the important catalytic residues in position to maintain their respective interactions (Figure 3C). One minor difference is an ∼1 Å movement of residue N174 away from the abasic site 5′-phosphate. This movement disrupts the hydrogen bond between N174 and the bridging oxygen of the cleaved abasic site that is observed in the APE1:dsDNA structure. The subtle rearrangement of N174 likely reduces the stability of the abasic site and may contribute to the observed decrease in APE1 activity on ssDNA substrates. Together, this structure suggests APE1 utilizes the same active site residues and catalytic mechanism for processing ssDNA and dsDNA abasic sites.

Characterization of APE1 residue R177 during cleavage of abasic sites in ssDNA

In addition to the active site catalytic residues, we examined the roles of the APE1 DNA intercalating residue, R177. Structurally, R177 intercalates between the two strands of double stranded DNA (Figure 4A). In this position, R177 acts as a surrogate base by intercalating into the major groove and forming base stacking interactions (49). Additionally, R177 acts as a block between the abasic site and the orphan base, so they cannot hydrogen bond and the abasic site can be flipped out of the dsDNA into the active site for proper catalytic alignment. One unique property of APE1 processing ssDNA substrates is that there is no opposing non-damaged strand of DNA that must be held away from the abasic site strand during cleavage (Figure 4B). To determine if R177 is involved in processing of ssDNA substrates, we completed pre-steady-state kinetic analysis of the R177A mutant with each DNA substrate (Figure 4C and D). For the PTJ substrate, the k_{obs} and k_{ss} were determined to be 0.23 ± 0.03 and 0.07 ± 0.003 s^{-1}, respectively. Compared to WT APE1, this represents a 43.5-fold decrease in catalysis and a 38.6-fold decrease in product release. For the recessed PTJ substrate, which has the abasic site further removed from the double stranded junction, k_{obs} was 0.12 ± 0.015 s^{-1} and k_{ss} was 0.06 ± 0.006 sec^{-1}, representing a 250-fold decrease in catalysis and 98.3-fold decrease in product release (Figure 4C and Table 2). Finally, for the ssDNA substrate, k_{obs} was determined to 0.001 ± 0.0001 and the k_{ss} 0.0001 ± 0.000008 s^{-1}, representing a 2000- and 1500-fold decrease, respectively (Figure 4D and Table 2). Together, these data indicate that R177 serves an important function in APE1 catalysis of ssDNA that is unique from its activity on dsDNA. We propose that R177A stabilizes the bases flanking the abasic site to provide stability to the base stacking of the DNA in the absence of a complimentary DNA strand.

As seen in the WT kinetics for both PTJ substates, k_{obs} is <10-fold greater than the k_{ss} value, which makes accurate determination of k_{obs} difficult. To confirm the reported k_{obs} for both PTJ substrates, we preformed additional single-turnover kinetic measurements with the R177A mutant. As observed previously with abasic dsDNA single-turnover kinetics, curves are best fit with a double exponential equa-

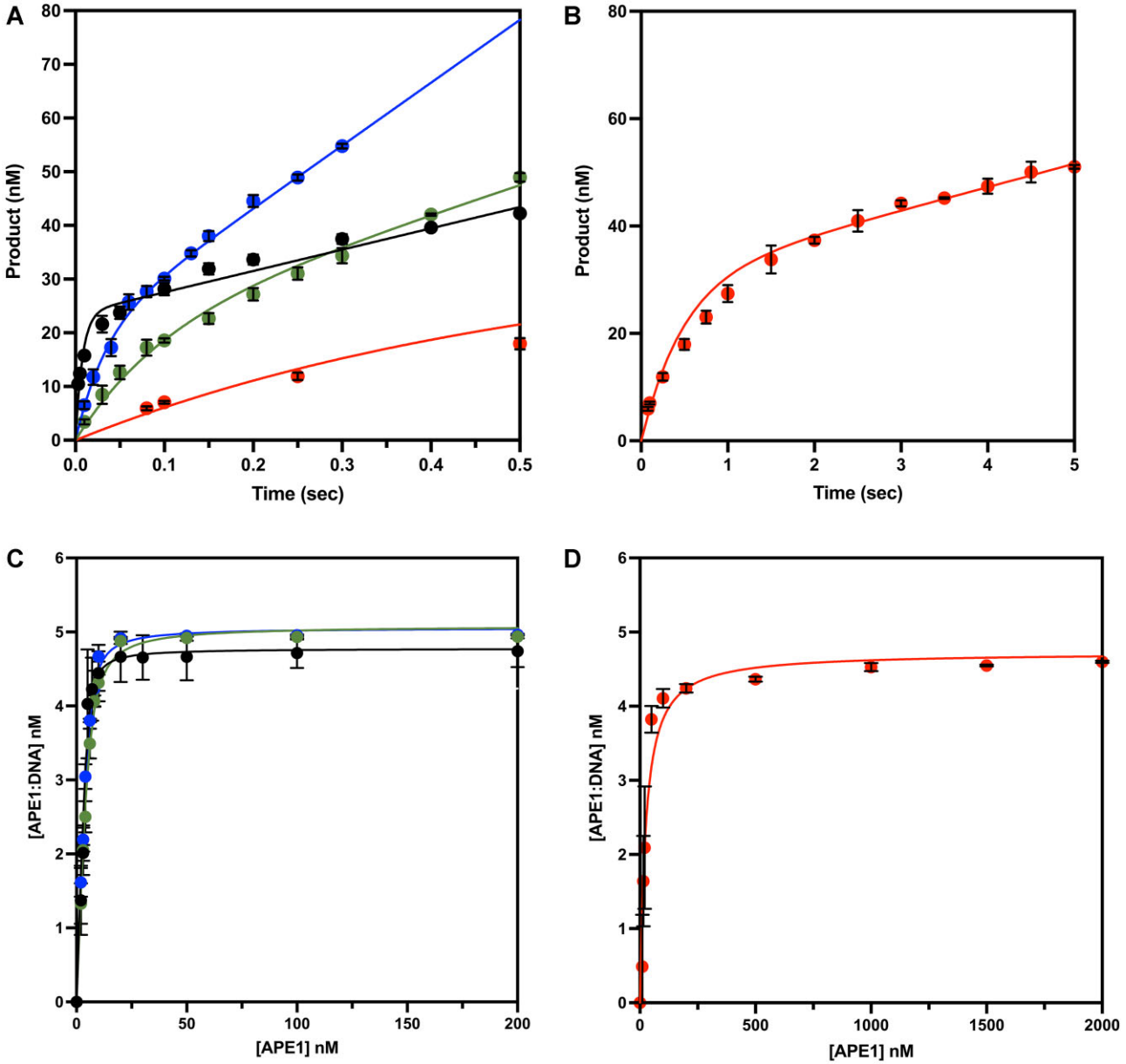

Figure 2. Cleavage activity and binding of wild-type APE1 with PTJ and ssDNA substrates. (**A**) Multiple turnover kinetic (DNA at 100 nM and APE1 at 30 nM) time courses of product formation for the reaction with line of best fit for each substrate; dsDNA (black), PTJ (green), Recessed PTJ (blue), and ssDNA (red). (**B**) Extended time points for the ssDNA kinetic curve (red). (**C**) Quantification of EMSA analysis (DNA at 5 nM, APE1 at 0–200/2000 nM). The line represents best fit to Equation (1) for; dsDNA (black), PTJ (green), and Recessed PTJ (blue). (**D**) Extended points for ssDNA EMSA curve (red). All points are shown as the mean of three independent experiments with error bars (st. dev.) shown. Where error bars are not seen, they are smaller than the data point.

Table 2. Pre-steady-state (multiple turnover) kinetic parameters of the APE1 R177A (DNA at 100 nM, APE1 at 30 nM). Wild-type values are the same as those shown in Table 1 for comparison to R177A values. Fold change is calculated for each substrate using the corresponding wild-type value

APE1	Substrate	k_{obs} (s^{-1})	k_{obs} (fold change)	k_{ss} (s^{-1})	k_{ss} (fold change)
WT	PTJ	10 ± 1	–	2.7 ± 0.21	–
R177A	PTJ	0.23 ± 0.03	43.5 ± 6.9	0.07 ± 0.003	38.6 ± 3.4
WT	Rec PTJ	30 ± 4	–	5.9 ± 0.32	–
R177A	Rec PTJ	0.12 ± 0.015	250 ± 45.5	0.06 ± 0.006	98.3 ± 2.5
WT	ssDNA	2 ± 0.2	–	0.15 ± 0.018	–
R177A	ssDNA	0.001 ± 0.0001	2000 ± 280	0.0001 ± 0.000008	1500 ± 216

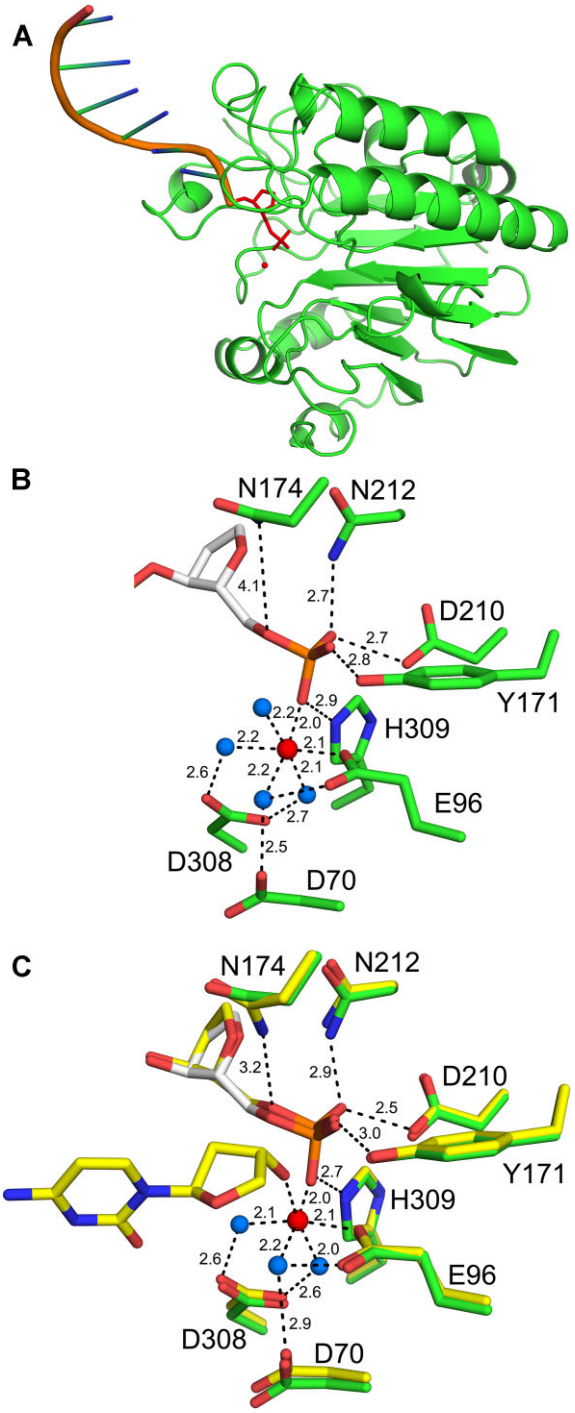

Figure 3. High-resolution structure of APE1: ssDNA product complex. (**A**) Overview of the APE1:ssDNA structure with APE1 (green, ribbons) and ssDNA (orange, cartoon). (**B**) A focused view of the APE1 active site with the THF (white) and key residues (green) shown in stick format (with distances in Å). The catalytic metal and active site waters are shown as red and blue spheres, respectively. (**C**) Overlay of ssDNA (green) with previous structure for WT APE1 bound abasic dsDNA (yellow, PDB: 5DFF). The catalytic metal, active site waters, and distances (Å) correspond to the dsDNA structure (PDB: 5DFF).

tion, indicating the presence of two distinct cleavage rates (41). Here, we will focus our discussion on the rate determined for the major population for each substrate. The single turnover k_{obs} for the PTJ and Rec-PTJ substrates were determined to be 0.05 ± 0.004 and 0.06 ± 0.006 s^{-1}, respectively (Supplementary Figure S7). In this case, since the single turnover k_{obs} values are similar to the determined k_{ss} values, single turnover measurements provide a more accurate rate than multiple turnover measurements. However, both values emphasize the drastic reduction in activity observed for the R177A mutant from WT rates, highlighting this residue's importance.

APE1 exchange for RPA on abasic PTJ substrates

At a stalled replication fork, exposed single stranded DNA is bound by the major ssDNA binding protein, RPA. The concentration of RPA is $\sim 1 \times 10^5$ molecules per cell and similar to that of APE1 (51). Additionally, it was recently shown that APE1 can interact with RPA (52,53). To study the interplay between RPA and APE1 on our PTJ substrates, we employed a novel FRET assay. This assay utilizes Cy5-labeled RPA and Cy3-labeled PTJ DNA substrates that contain an abasic site either directly next to the junction (PTJ) or 7 nucleotides away (Rec-PTJ), as used in the kinetic assays presented previously. The primer has a Cy3 FRET donor attached at the 3′ terminus. The length (33 nt) of the 5′ ssDNA overhang accommodates one RPA heterotrimeric complex (54–57) (Figure 5A). In mass photometry analysis of a PTJ DNA substrate containing a 30 nt 5′ ssDNA overhang, only one RPA is bound to the DNA in nearly all (∼90%) complexes, even when a three-fold molar excess of RPA is present in the reaction (Supplementary Figure S5). The RPA complex is labeled with a Cy5 FRET acceptor at position 107 of the RPA32 subunit, which lies within OB-fold D (40) (Figure 5B). RPA resides on the 5′ ssDNA overhang with specific polarity such that the Cy5-labeled DBD-D is oriented towards the Cy3-labeled PTJ (40,58) (Figure 5C and D). With RPA titration, the FRET signal increases linearly due to direct protein•DNA interactions (rather than indirect buffer or dilution effects) and then reaches a plateau after which the FRET signal remains constant (Supplementary Figures S8–S10). Altogether, this indicates that both DNA substrates can be saturated with Cy5-RPA. In the APE1 experimental samples (Figure 6A), Cy3-labeled Rec-PTJ is pre-saturated with Cy5-labeled RPA, yielding a high FRET state, and the resultant mixture is then titrated with catalytically dead APE1 (i.e. $APE1_{Dead}$). E_{FRET} is calculated after each addition of $APE1_{Dead}$. Under the conditions of the assay, a decrease in E_{FRET} indicates that $APE1_{Dead}$ engages the DNA and either: (i) alters the configuration of the RPA complex on DNA such that the distance between the FRET dyes increases (yielding an intermediate FRET state); (ii) displaces RPA from the DNA (yielding a low FRET state) or (iii) a combination of both possibilities. For both the PTJ and Rec-PTJ substrates, formation of the DNA-RPA complex is indicated by a robust FRET signal before $APE1_{Dead}$ is added.

For the Rec-PTJ substrate (Figure 6B), which contains an abasic site 7 nucleotides downstream of the PTJ, a robust

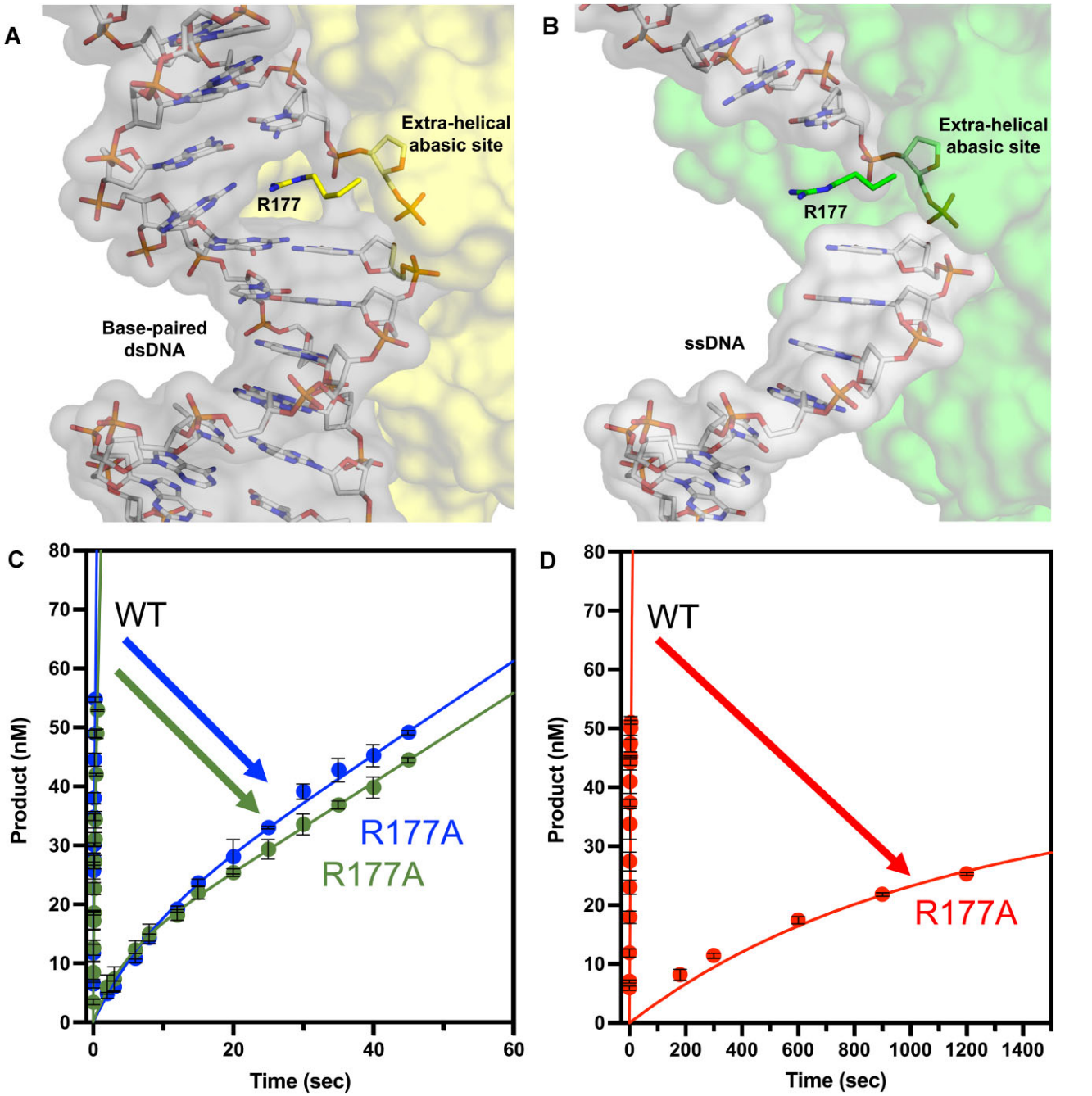

Figure 4. APE1 R177A mutant activity. (**A**) APE1 (yellow, surface) bound to product dsDNA (sticks and grey surface) highlighting DNA intercalating residue R177 (yellow, sticks) (PDB: 5DFF). (**B**) APE1 (green, surface) bound to ssDNA with downstream strand modeled from PDB 5DFF highlighting R177 (green, sticks). Multiple turnover kinetic time courses (DNA at 100 nM, APE1 at 30 nM) of product formation for (**C**) PTJ (green) and Recessed PTJ (blue) and (**D**) ssDNA (red) substrates with line of best fit (in corresponding colors) compared to wild type (WT). All time points are shown as the mean of three independent experiments with error bars (st. dev.) shown. Where error bars are not seen, they are smaller than the data point.

FRET signal is observed prior to the addition of $APE1_{Dead}$ (High FRET, Cy5-RPA Bound). Over the course of the $APE1_{Dead}$ titration, the observed E_{FRET} values decrease to within experimental error of the low FRET state where the DNA substrate is devoid of RPA. This indicates complete exchange of RPA for $APE1_{Dead}$ on the Rec-PTJ DNA substrate. The intermediate FRET values observed during the titration may represent RPA binding in different conformations before its complete exchange at the high APE1 concentrations. In the FRET assay, it was necessary to use catalytically dead APE1 to prevent cleavage from occurring, however it is also of interest to determine if APE1 is able to cut the DNA substrate under these experimental conditions. To test APE1 activity, we analyzed APE1 product formation under the same experimental conditions and protein ratios as the FRET experiments. The product formation as-

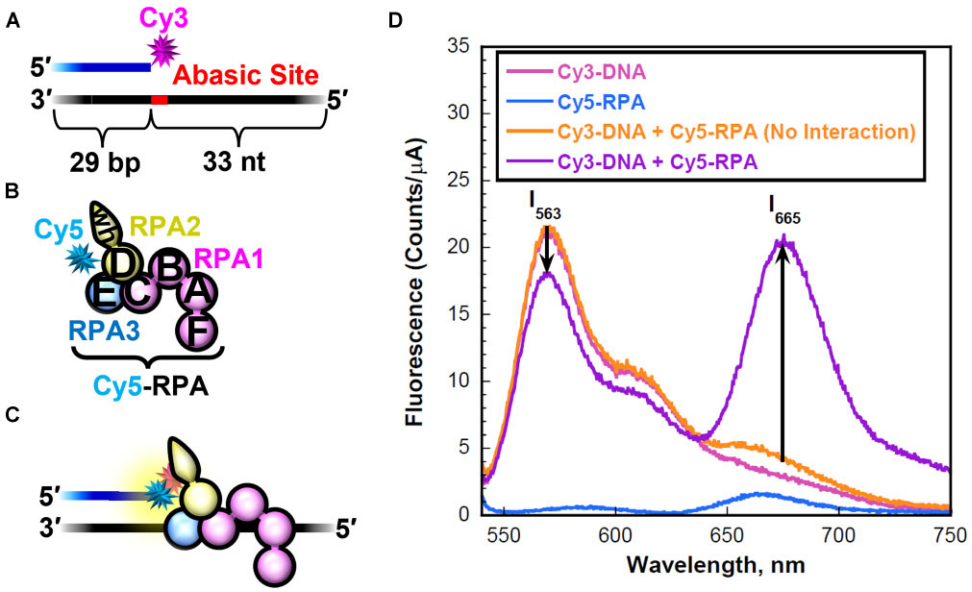

Figure 5. RPA engaging a PTJ that contains an abasic site. (**A**) Schematic representation of the 3′ Cy3-labeled PTJ substrate (also depicted in Supplementary Figure S2A). (**B**) Schematic representation of Cy5-labeled RPA. The RPA subunits are color-coded (RPA1 in pink, RPA2 in yellow, and RPA3 in blue) and depicted to illustrate the OB-folds (A–E) and winged-helix (wh) domain. The RPA complex is labeled with a Cy5 FRET acceptor at residue 101 of the RPA32 subunit. This position lies within OB-fold D. (**C**) Schematic representation of RPA interactions at a PTJ. RPA interacts with the 5′ ssDNA overhang in an orientation-specific manner such that the Cy5-labeled RPA32 subunit is oriented towards the Cy3-labeled PTJ. (**D**) Fluorescence emission spectra (540–750 nm) obtained by exciting the Cy3-labeled PTJ DNA (25 nM) with 514 nm light. The fluorescence emission intensities (*I*) at 665 nm (Cy5 FRET acceptor fluorescence emission maximum, I_{665}) and 563 nm (Cy3 FRET donor fluorescence emission maximum, I_{563}) are indicated. Cy5-labeled RPA (75 nM) can be excited via FRET from Cy3 only when the two fluorophores are in close proximity (i.e. <10 nm). This is indicated by an increase in I_{665} and a concomitant decrease in I_{563}. The predicted spectrum for no interaction between RPA and DNA is determined by adding the spectrums of the individual components.

say demonstrates that at a [APE1]/[DNA] = 1, about 25% product was generated after only 30 seconds and increasing product was generated over time (Figure 6C). As expected, we observe an APE1 concentration-dependent increase in activity. Compared to the no RPA control, this represents a decrease in APE1 activity in presence of RPA, which is consistent with previous publications reporting RPA suppressing APE1 activity (30) (Figure 6D). However, this data demonstrates that APE1 maintains robust cleavage activity even in the presence of RPA.

For the PTJ substrate, where the PTJ directly abuts an abasic site, the observed E_{FRET} values do not change over the course of the $APE1_{Dead}$ titration. This indicates that $APE1_{Dead}$ does not exchange for RPA nor promote a long-lived conformational re-arrangement of RPA that increases the distance between the FRET dyes (Figure 7A and B). However, it should be noted that we cannot rule out that $APE1_{Dead}$ engages RPA-bound DNA in a manner that does not alter the distance between the FRET dyes. Thus, at least DBD-D (and likely DBD-E) of the RPA complex remain stably bound to the PTJ even at very high concentrations of $APE1_{Dead}$. Remarkably, product formation assays reveal that APE1 is able to cleave the abasic DNA under these conditions. As seen for the Rec-PTJ, we observe increasing APE1 activity over time and with increasing APE1 concentrations (Figure 7C and D). This data demonstrates that APE1 is active on the abasic PTJ substrate with RPA still bound to the DNA. It is likely that APE1 is cutting both the Rec-PTJ and the PTJ substrates while RPA is bound, however in the Rec-PTJ the position of the abasic site is allowing APE1 to kick RPA off the substrate at very high APE1 concentrations.

To account for the position of the abasic site in the PTJ substrates, we used competitor DNA to determine the relative binding affinity of RPA for each substrate. When the unlabeled competitor DNA is identical to the Cy3-labeled DNA substrate on which the FRET complex is formed, it is expected that 50% inhibition is observed when the concentration of competitor DNA is equal to the concentration of the substrate DNA, i.e. $[\text{Competitor DNA}]/[\text{DNA}]_{Total} = 0.50$. Using Cy3-labeled Rec-PTJ and unlabeled competitor Rec-PTJ DNA, the observed $[\text{Competitor DNA}]/[\text{DNA}]_{Total}$ is equal to $0.487 \pm 5.61 \times 10^{-3}$, confirming the validity of the approach and that the Cy3 label at the PTJ has no effect on the binding of RPA to the DNA substrates (Supplementary Figure S11). When the competitor DNA is instead the PTJ DNA substrate (contains an abasic site at the PTJ) the observed $[\text{Competitor DNA}]/[\text{DNA}]_{Total}$ decreases slightly to 0.413 ± 0.0447, indicating that RPA has a slightly higher relative affinity for a PTJ substrate compared a Rec-PTJ substrate (Supplementary Figure S11). However, this slight difference in affinities does not account for the drastic difference in RPA/APE1 exchange for the PTJ and Rec-PTJ DNA substrates (Figures 6B and 7B). Hence, the observed differences in exchange of APE1 for RPA on the PTJ DNA substrates are likely attributed to differential dynamics of RPA on the abasic site-containing PTJ DNAs.

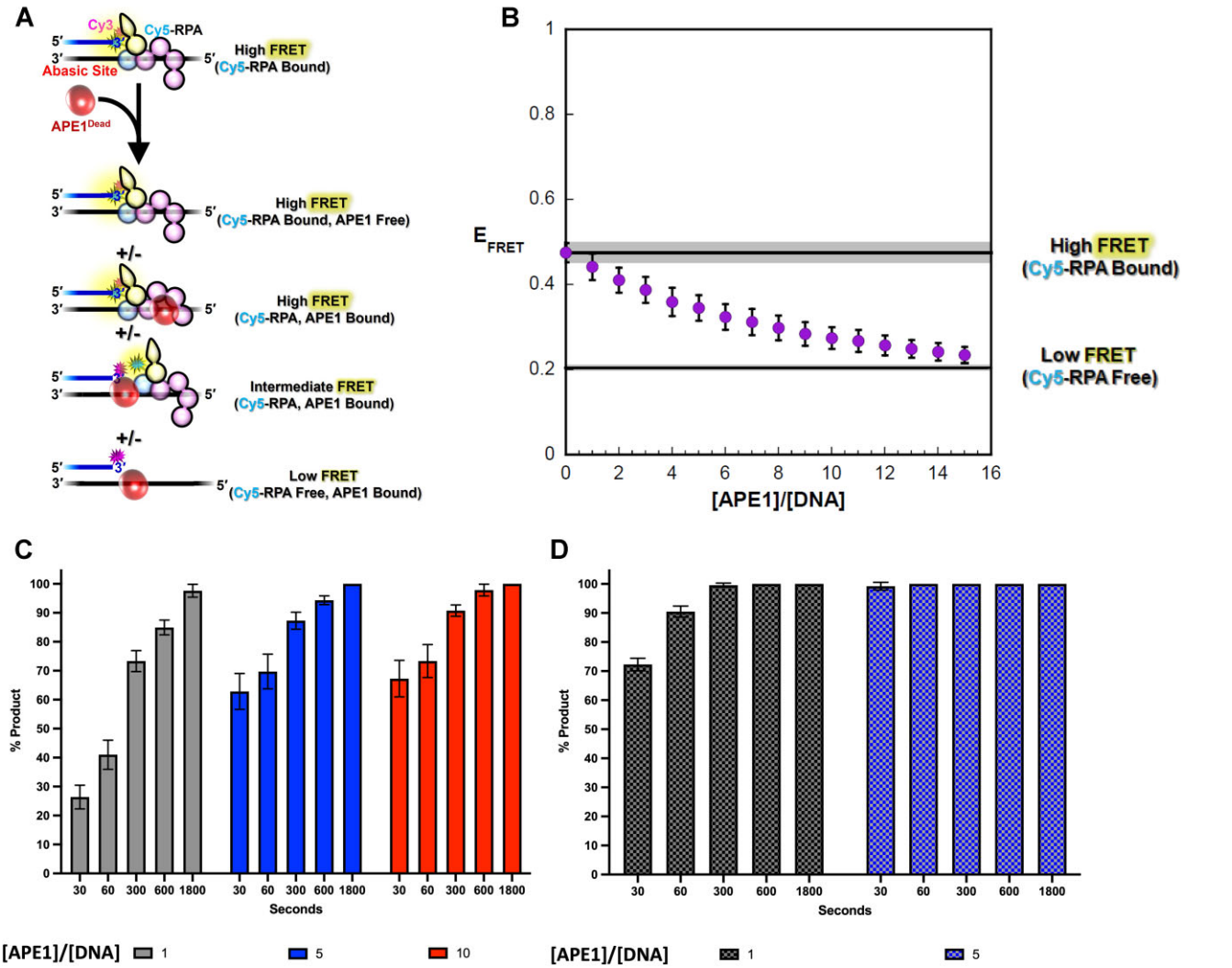

Figure 6. RPA/APE1 exchange on the Rec-PTJ substrate. (**A**) Schematic representation of the FRET experiment. A 3′ Cy3-labeled Rec-PTJ DNA containing an abasic site 7 nt downstream of the PTJ (25 nM, 3 pmol, Supplementary Figure S2A) is pre-saturated with Cy5-labeled RPA (75 nM), yielding a high FRET state, (Supplementary Figure S8) and the resultant mixture is then titrated with catalytically dead APE1 (i.e. $APE1_{Dead}$). E_{FRET} is calculated after each addition of protein. The ssDNA downstream of the PTJ (33 nt) can accommodate a single Cy5-RPA or 3 $APE1_{Dead}$. Possible protein•DNA complexes and their expected E_{FRET} values are depicted. (**B**) E_{FRET} values are plotted as a function of [$APE1_{Dead}$]/[DNA] ratio and each data point represent the mean ± S.E.M. of at least three independent measurements. The E_{FRET} value observed in the absence of $APE1_{Dead}$ (0.475 ± 0.0227) is extrapolated to the axis limits as a flat black line (with S.E.M. displayed in grey) to indicate the high FRET state where the DNA substrate is devoid of $APE1_{Dead}$. The predicted E_{FRET} value for no interaction between RPA and DNA (0.204 ± 0.00394) is displayed as a flat black line (with S.E.M. displayed in grey) to indicate the low FRET state where the DNA substrate is devoid of RPA. The observed FRET decreases to within experimental error of the low FRET state over the range of $APE1_{Dead}$ additions, indicating that $APE1_{Dead}$ completely exchanges for RPA. (**C**) Ape1 product formation (%) values over time with Rec-PTJ substrate (100 nM) pre-saturated RPA (200 nM). (**D**) Ape1 product formation (%) in absence of RPA on Rec-PTJ substrate. [$APE1_{Dead}$]/[DNA] ratio of 1, 5 and 10 indicated by color as grey, red and blue, respectively with each bar representing the mean ± S.E.M. of at least three independent measurements.

DISCUSSION

APE1 cleavage of ssDNA substrates

Previous work has demonstrated APE1 cleavage activity on several complex structures, such as various duplexes, bubbles, and forks (29,30,59,60). Here, we advance our understanding of this APE1 activity using pre-steady-state kinetics, binding, and X-ray crystallography to determine how APE1 processes ssDNA abasic sites in substrates that represent aspects of a stalled replication fork. Data demonstrate that APE1 binds these substrates with high affinity and cleaves with only moderately reduced activity compared to canonical APE1 cleavage of double stranded DNA substrates. The kinetic values of APE1 cleavage are well within the range of reported rates for other APE1 substates, as well as other DNA repair enzyme activities (36,61–66). It has been previously observed that some form of DNA secondary structure is preferred for APE1 activity, but that proximity of the abasic site influences APE1 incision efficiency (30). Our data supports this observation, as APE1 cleavage efficiency is affected by the position of the abasic site compared to the double stranded PTJ.

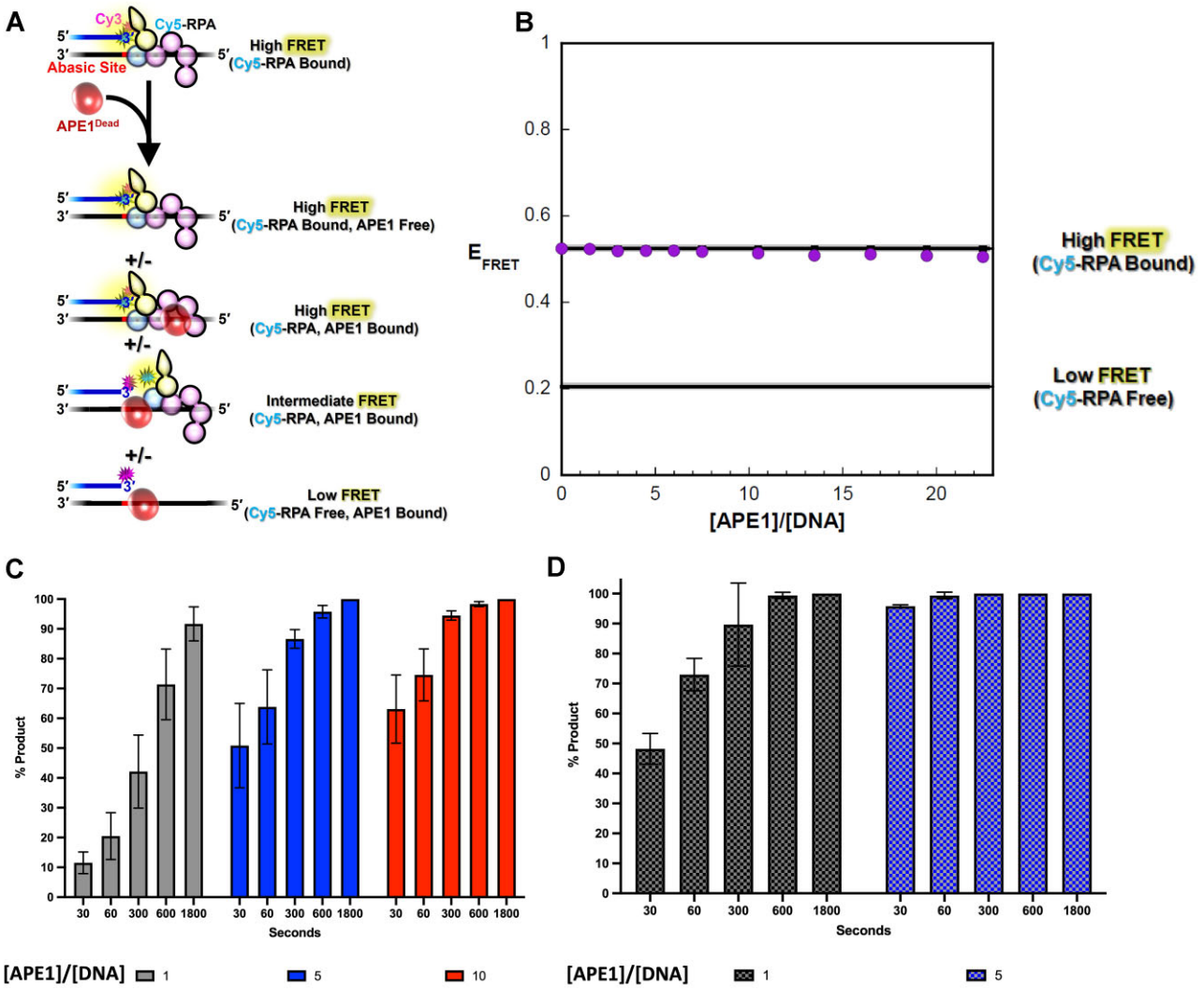

Figure 7. RPA/APE1 exchange on the PTJ substrate. (**A**) Schematic representation of the FRET experiment. A 3′ Cy3-labeled PTJ DNA containing an abasic site at the PTJ (25 nM, 3 pmole, Supplementary Figure S2A) is pre-saturated with Cy5-labeled RPA (75 nM) (Supplementary Figure S9), yielding a high FRET state, and the resultant mixture is then titrated with catalytically dead APE1 (i.e. $APE1_{Dead}$). E_{FRET} is calculated after each addition of protein. The ssDNA downstream of the PTJ (33 nt) can accommodate a single Cy5-RPA or 3 $APE1_{Dead}$. Possible protein•DNA complexes and their expected E_{FRET} values are depicted. (**B**) E_{FRET} values are plotted as a function of [APE1Dead]/[DNA] ratio and each data point represent the mean ± S.E.M. of four independent measurements. The E_{FRET} value observed in the absence of $APE1_{Dead}$ (0.524 ± 0.00608) is extrapolated to the axis limits as a flat black line (with S.E.M. displayed in grey) to indicate the high FRET state where the DNA substrate is devoid of $APE1_{Dead}$. The predicted E_{FRET} value for no interaction between RPA and DNA (0.205 ± 0.00538) is displayed as a flat black line (with S.E.M. displayed in grey) to indicate the low FRET state where the DNA substrate is devoid of RPA. The observed FRET does not decrease over the range of protein additions, indicating that RPA is not exchanged for APE1. (**C**) Ape1 product formation (%) values over time with PTJ substrate (100 nM) pre-saturated RPA (200 nM). (**D**) Ape1 product formation (%) in absence of RPA on PTJ substrate. [$APE1_{Dead}$]/[DNA] ratio of 1, 5 and 10 indicated by color as grey, red, and blue, respectively with each bar representing the mean ± S.E.M. of at least three independent measurements.

There is growing evidence for APE1 nuclease activity on a variety of non-canonical, biologically relevant, nucleic-acid substrates, beyond abasic sites within B-form duplex DNA (28–30,41,59,60,67–72). While it is difficult to compare kinetic rates on various substrates directly, due to different assay conditions, there is an overarching theme emerging that APE1 must bind and accommodate an array of diverse nucleic-acid substrates using its single active site. This was originally proposed to occur through a DNA sculpting mechanism, where structural changes of the nucleic-acid substrates are imposed by APE1 binding (43,73). Among the nucleases in a cell, DNA repair nucleases are unique because they lack sequence specificity (74–79). These 'structure-specific' nucleases, such as APE1, must use the nucleic-acid structure, rather than a specific sequence, to control their recognition and provide specificity to their damaged substrates. The term 'DNA sculpting' has been used to describe the bending and shaping of DNA substrates by repair enzymes. As such, when a protein-DNA complex is formed, changes are observed in DNA structure as opposed to the protein active site. Numerous published structures have observed the APE1 active site to be very rigid with few significant changes seen among a variety of bound substrates (36,43,49). Therefore, if APE1

can sculpt the substrate into its relatively rigid active site, it can efficiently catalyze cleavage using the same catalytic residues and nucleophilic attack mechanism. We anticipate this sculpting mechanism that is utilized to bind nucleic-acid substrates in a catalytically competent position, will apply to the other complex nucleic acid structures.

R177 is critical to APE1 ssDNA cleavage activity

Since the first structural observations of APE1 residue R177 intercalating dsDNA, this residue has been of interest in the APE1 field (43). Today, R177 has been implicated in several functions in the APE1 catalytic mechanism including product release, protein-DNA interactions, and substrate specificity (36,43,49,80–82). Mutation of R177 to alanine results in only subtle increases in kinetic rate for both the AP-endonuclease and proofreading exonuclease activities (36,49). However, a recent publication reported that R177A decreased APE1 activity when processing a 3′-8oxoG lesion, indicating R177 plays an important role in mechanism of 8oxoG processing by APE1 (83).

Previous APE1 R177 descriptions all include APE1 interacting with both strands of dsDNA substates, prompting our interest in the function of residue R177 in the context of ssDNA substrates. The R177A mutation resulted in reduced APE1 kinetic rates on all three of the PTJ and ssDNA substrates. In fact, kinetic data indicates that the R177 side chain becomes more critical for APE1 activity as the amount of flanking dsDNA decreases (as demonstrated by lowest rate for ssDNA, Table 2). Based on the data presented here, we propose that R177 plays a role in stabilizing the bases flanking the abasic site to provide stability to the base stacking of the DNA in the absence of a complimentary DNA strand. Additionally, it is likely that R177 is playing a 'space filling role' acting as a physical block to hold the abasic site out of the double helix and into the active site for cleavage, similar to the role described as the 'RM bridge' (81). These experiments, along with structural observations, provide insight into why R177 may have a more critical role in APE1 cleavage of ssDNA over its modest role observed for canonical APE1 function processing dsDNA.

APE1:DNA interactions

Although there is currently no structure of APE1 bound to a primer template junction substrate, structural data presented here provide insight into the expected interactions between APE1 and a PTJ. APE1 interactions with double stranded DNA have been classified into two regions or 'hot spots' (Supplementary Figure S12A) (81). These two regions are (1) with the abasic strand backbone flanking the cleavage site and (2) with the opposing nondamaged strand backbone downstream (3′) of the orphan base (Supplementary Figure S12A). The latter of these interaction hot spots would be lost in an APE1-PTJ interaction, as the 3′ region of the nondamaged strand would be missing from a PTJ structure (Supplementary Figure S12A, cyan bracket). Alternatively, when interacting with a ssDNA-dsDNA PTJ, APE1 may utilize a novel, and currently unknown, mode of binding to facilitate catalysis.

The interaction schematic highlights that the majority of APE1 interactions are with the abasic strand of DNA (Supplementary Figure S12B). In this way, APE1 approaches the DNA from the damaged side and 'sits' on the abasic strand. Unlike polymerases, which use the templating strand for insertion, APE1 does not rely on the opposing strand for activity, and is thus capable of cleaving ssDNA substrates, as demonstrated by the data presented in this study. Furthermore, APE1 does not make significant contacts with the damaged strand 5′ of the active site (Supplementary Figure S12A, pink bracket), as demonstrated in substrate complex (PDB: 5DFI), product complex (PDB: 5DFF), as well as the loss of this strand in the APE1:ssDNA product complex structure presented here (Figure 3A) (84). In a cellular context, this would present a biological problem if APE1 cuts the backbone of a ssDNA substrate and immediately loses contact with this portion of the DNA. In this way, APE1 cleavage could instantly collapse the replication fork, potentially even while APE1 is still bound. One hypothesis is that fragile repair intermediates are protected during repair through substrate channeling among repair enzymes. Therefore, other enzymes are likely needed to protect such a repair intermediate for other pathways that are necessary for repair. Alternatively, APE1 cleavage of ssDNA may be very deleterious to the cell, and therefore depend heavily on proteins to protect abasic ssDNA from APE1 cleavage.

Interplay between APE1 and RPA

When a DNA polymerase stalls at a lesion, the DNA helicase continues to unwind dsDNA generating stretches of excess ssDNA which are then coated by RPA (8,9,85–87). By binding transiently exposed ssDNA, RPA serves as a hub protein to coordinate DNA replication, as well as other cellular processes (51,88). RPA binds to ssDNA with a subnanomolar affinity; however, the RPA-ssDNA complex is dynamic, and several studies have suggested the RPA DNA-binding domains (DBDs) undergo microscopic dissociations from the ssDNA (54,89,90). These microscopic dissociations from the DNA are thought to enable lower affinity DNA-binding proteins to displace and/or remodel RPA.

Here, we observe that APE1 is able to cleave the phosphodiester backbone of an abasic PTJ substrate while RPA remains bound. In this way, APE1 and RPA are accommodated on the same DNA substrate. Furthermore, when the abasic site is positioned further from the PTJ in the ssDNA region, APE1 is able to displace RPA at high concentrations. This is consistent with a dynamic RPA-DNA complex allowing APE1 to interact with exposed DNA or during microscopic dissociation events. While RPA does have a large interaction 'footprint' with the DNA (18–22 nt), structural remodeling or basal diffusion of RPA exposes stretches of ssDNA and likely allows APE1 to gain access to a lesion for rapid cleavage. Data reported here supports a dynamic RPA-DNA complex which allows access to other DNA repair factors, such as APE1. This model is further supported by recent work that demonstrated RPA DBD-A and DBD-B are dynamic and that the RPA–ssDNA complex exists in at least four distinct conformations that each allow varying access to the ssDNA (91). Similarly, the interaction of RPA with uracil DNA glycosylase (UNG) was shown to stimu-

late the excision of uracil from RPA-coated ssDNA via increased accessibility of ssDNA (17).

RPA has high affinity for ssDNA, even with an abasic site, and thus coats ssDNA upon its exposure. In addition, using Xenopus egg extracts it was recently determined that the RPA32 subunit interacts with APE1 through the N-terminal domain of APE1 (52,53). Furthermore, this interaction may facilitate the interaction of APE1 with ssDNA through a mechanism that is not fully understood. Together, this raises the question as to how these two powerhouse proteins interface at a ssDNA abasic site. RPA has been observed to inhibit APE1 ssDNA cleavage activity under certain experimental conditions (30). Consistently, we observed a reduction in APE1 product formation in the presence of RPA. However, it is important to consider the abundance of cellular APE1 (0.35 to 7 $\times$ 10^6 molecules per cell), which was not accounted for in previous experiments. We observed that even with RPA pre-saturated on the DNA, APE1 has a robust cleavage activity over a range of APE1 concentrations. This validates that APE1 is not completely inhibited by the presence of RPA but is in fact still capable of enzymatic cleavage. It is possible that RPA-coated ssDNA could inhibit APE1 binding or alter ssDNA structural elements necessary for APE1 activity. However, the kinetic rates determined here identify that APE1 rapidly cleaves abasic sites in these DNA substrates that contain ssDNA, even in the presence of RPA. Importantly, APE1 cleavage of RPA-coated ssDNA containing abasic sites at the replication fork would have significant implications for genomic stability, as it would generate a double stranded break that could collapse the replication fork. This suggests that cellular mechanisms likely exist to prevent APE1 cleavage of ssDNA or to protect the nicked ssDNA following APE1 cleavage. Further work is needed to elucidate the complex interplay between APE1 and RPA, as well as to determine what additional factors are involved in processing abasic sites at the replication fork.

DATA AVAILABILITY

Atomic coordinates and structure factors for the reported crystal structure have been deposited with the Protein Data Bank under accession number 7TR7.

SUPPLEMENTARY DATA

Supplementary Data are available at NAR Online.

ACKNOWLEDGEMENTS

We would like to thank Dr Tyler Weaver for his input and assistance during the revision of this manuscript.
Author contributions: B.D.F. and N.M.H. designed the study. N.M.H., J.L.N., V.K. and R.C. expressed and purified the proteins. T.H.K. collected the crystal structure. N.M.H. performed kinetic and binding data acquisition, X-ray crystallographic structure refinement/deposition. M.H. designed the FRET experiments. J.L.N., V.K. and R.C. performed the FRET experiments. B.D.F., M.H., E.A. and N.M.H analyzed data and wrote the manuscript.

FUNDING

National Institute of Environmental Health Sciences [R01ES029203 to B.D.F.]; National Institute of General Medical Science [R01GM133967, R01GM130746 to E.A., 1R35GM147238-01 to M.H.] of the National Institutes of Health; American Heart Association [20PRE35210752 to N.M.H.]; A.U.C. experiments to characterize the fluorescent human RPA were supported by a grant from the National Instituted of Health [S10OD030343 to EA]. Funding for open access charge: National Institute of Environmental Health Sciences [R01ES029203 to B.D.F.].
Conflict of interest statement. None declared.

REFERENCES

1. De Bont,R. and van Larebeke,N. (2004) Endogenous DNA damage in humans: a review of quantitative data. *Mutagenesis*, **19**, 169–185.
2. Loeb,L.A. and Preston,B.D. (1986) Mutagenesis by apurinic/apyrimidinic sites. *Annu. Rev. Genet.*, **20**, 201–230.
3. Lindahl,T. and Nyberg,B. (1972) Rate of depurination of native deoxyribonucleic acid. *Biochemistry*, **11**, 3610–3618.
4. Barnes,D.E. and Lindahl,T. (2004) Repair and genetic consequences of endogenous DNA base damage in mammalian cells. *Annu. Rev. Genet.*, **38**, 445–476.
5. Schaaper,R.M., Kunkel,T.A. and Loeb,L.A. (1983) Infidelity of DNA synthesis associated with bypass of apurinic sites. *Proc. Natl. Acad. Sci. U.S.A.*, **80**, 487–491.
6. Lockhart,M.L., Deutsch,J.F., Yamaura,I., Cavalieri,L.F. and Rosenberg,B.H. (1982) Termination of DNA synthesis in vitro at apurinic sites but not at ethyl adducts on the template. *Chem. Biol. Interact*, **42**, 85–95.
7. Sagher,D. and Strauss,B. (1983) Insertion of nucleotides opposite apurinic/apyrimidinic sites in deoxyribonucleic acid during in vitro synthesis: uniqueness of adenine nucleotides. *Biochemistry*, **22**, 4518–4526.
8. Smith,K.D., Fu,M.A. and Brown,E.J. (2009) Tim-Tipin dysfunction creates an indispensible reliance on the ATR-Chk1 pathway for continued DNA synthesis. *J. Cell Biol.*, **187**, 15–23.
9. Van,C., Yan,S., Michael,W.M., Waga,S. and Cimprich,K.A. (2010) Continued primer synthesis at stalled replication forks contributes to checkpoint activation. *J. Cell Biol.*, **189**, 233–246.
10. Zellweger,R., Dalcher,D., Mutreja,K., Berti,M., Schmid,J.A., Herrador,R., Vindigni,A. and Lopes,M. (2015) Rad51-mediated replication fork reversal is a global response to genotoxic treatments in human cells. *J. Cell Biol.*, **208**, 563–579.
11. Jackson,J. and Vindigni,A. (2022) Studying single-stranded DNA gaps at replication intermediates by electron microscopy. *Methods Mol. Biol.*, **2444**, 81–103.
12. Cong,K., Peng,M., Kousholt,A.N., Lee,W.T.C., Lee,S., Nayak,S., Krais,J., VanderVere-Carozza,P.S., Pawelczak,K.S., Calvo,J. *et al.* (2021) Replication gaps are a key determinant of PARP inhibitor synthetic lethality with BRCA deficiency. *Mol. Cell*, **81**, 3128–3144.
13. Chastain,P.D., Nakamura,J., Rao,S., Chu,H., Ibrahim,J.G., Swenberg,J.A. and Kaufman,D.G. (2010) Abasic sites preferentially form at regions undergoing DNA replication. *FASEB J.*, **24**, 3674–3680.
14. Lindahl,T. (1979) DNA glycosylases, endonucleases for apurinic/apyrimidinic sites, and base excision-repair. *Prog. Nucleic Acid Res. Mol. Biol.*, **22**, 135–192.
15. Bhagwat,A.S., Hao,W., Townes,J.P., Lee,H., Tang,H. and Foster,P.L. (2016) Strand-biased cytosine deamination at the replication fork causes cytosine to thymine mutations in Escherichia coli. *Proc. Natl. Acad. Sci. U.S.A.*, **113**, 2176–2181.
16. Kavli,B., Otterlei,M., Slupphaug,G. and Krokan,H.E. (2007) Uracil in DNA–general mutagen, but normal intermediate in acquired immunity. *DNA Repair (Amst.)*, **6**, 505–516.
17. Kavli,B., Iveland,T.S., Buchinger,E., Hagen,L., Liabakk,N.B., Aas,P.A., Obermann,T.S., Aachmann,F.L. and Slupphaug,G. (2021) RPA2 winged-helix domain facilitates UNG-mediated removal of

uracil from ssDNA; implications for repair of mutagenic uracil at the replication fork. *Nucleic Acids Res.*, **49**, 3948–3966.
18. Harris,R.S. and Liddament,M.T. (2004) Retroviral restriction by APOBEC proteins. *Nat. Rev. Immunol.*, **4**, 868–877.
19. Mehta,K.P.M., Lovejoy,C.A., Zhao,R., Heintzman,D.R. and Cortez,D. (2020) HMCES maintains replication fork progression and prevents double-strand breaks in response to APOBEC deamination and abasic site formation. *Cell Rep.*, **31**, 107705.
20. Mohni,K.N., Wessel,S.R., Zhao,R., Wojciechowski,A.C., Luzwick,J.W., Layden,H., Eichman,B.F., Thompson,P.S., Mehta,K.P.M. and Cortez,D. (2019) HMCES maintains genome integrity by shielding abasic sites in single-strand DNA. *Cell*, **176**, 144–153.
21. Thompson,P.S. and Cortez,D. (2020) New insights into abasic site repair and tolerance. *DNA Repair (Amst)*, **90**, 102866.
22. Thompson,P.S., Amidon,K.M., Mohni,K.N., Cortez,D. and Eichman,B.F. (2019) Protection of abasic sites during DNA replication by a stable thiazolidine protein-DNA cross-link. *Nat. Struct. Mol. Biol.*, **26**, 613–618.
23. Halabelian,L., Ravichandran,M., Li,Y., Zeng,H., Rao,A., Aravind,L. and Arrowsmith,C.H. (2019) Structural basis of HMCES interactions with abasic DNA and multivalent substrate recognition. *Nat. Struct. Mol. Biol.*, **26**, 607–612.
24. Quinet,A., Tirman,S., Cybulla,E., Meroni,A. and Vindigni,A. (2021) To skip or not to skip: choosing repriming to tolerate DNA damage. *Mol. Cell*, **81**, 649–658.
25. Locatelli,G.A., Pospiech,H., Tanguy Le Gac,N., van Loon,B., Hubscher,U., Parkkinen,S., Syvaoja,J.E. and Villani,G. (2010) Effect of 8-oxoguanine and abasic site DNA lesions on in vitro elongation by human DNA polymerase in the presence of replication protein A and proliferating-cell nuclear antigen. *Biochem J.*, **429**, 573–582.
26. Villani,G., Hubscher,U., Gironis,N., Parkkinen,S., Pospiech,H., Shevelev,I., Cicco di,G., Markkanen,E., Syväoja,J.E. and Tanguy Le Gac,N. (2011) In vitro gap-directed translesion DNA synthesis of an abasic site involving human DNA polymerases epsilon, lambda, and beta. *J. Biol. Chem.*, **286**, 32094–32104.
27. Krokan,H.E. and Bjoras,M. (2013) Base excision repair. *Cold Spring Harb. Perspect Biol.*, **5**, a012583.
28. Whitaker,A.M. and Freudenthal,B.D. (2018) APE1: a skilled nucleic acid surgeon. *DNA Repair (Amst.)*, **71**, 93–100.
29. Marenstein,D.R., Wilson,D.M. 3rd and Teebor,G.W. (2004) Human AP endonuclease (APE1) demonstrates endonucleolytic activity against AP sites in single-stranded DNA. *DNA Repair (Amst.)*, **3**, 527–533.
30. Fan,J., Matsumoto,Y. and Wilson,D.M. 3rd (2006) Nucleotide sequence and DNA secondary structure, as well as replication protein A, modulate the single-stranded abasic endonuclease activity of APE1. *J. Biol. Chem.*, **281**, 3889–3898.
31. Thakur,S., Sarkar,B., Cholia,R.P., Gautam,N., Dhiman,M. and Mantha,A.K. (2014) APE1/Ref-1 as an emerging therapeutic target for various human diseases: phytochemical modulation of its functions. *Exp. Mol. Med.*, **46**, e106.
32. Chen,D.S., Herman,T. and Demple,B. (1991) Two distinct human DNA diesterases that hydrolyze 3′-blocking deoxyribose fragments from oxidized DNA. *Nucleic Acids Res.*, **19**, 5907–5914.
33. Beck,M., Schmidt,A., Malmstroem,J., Claassen,M., Ori,A., Szymborska,A., Herzog,F., Rinner,O., Ellenberg,J. and Aebersold,R. (2011) The quantitative proteome of a human cell line. *Mol. Syst. Biol.*, **7**, 549.
34. Parlanti,E., Locatelli,G., Maga,G. and Dogliotti,E. (2007) Human base excision repair complex is physically associated to DNA replication and cell cycle regulatory proteins. *Nucleic Acids Res.*, **35**, 1569–1577.
35. Kharat,S.S., Ding,X., Swaminathan,D., Suresh,A., Singh,M., Sengodan,S.K., Burkett,S., Marks,H., Pamala,C., He,Y. *et al.* (2020) Degradation of 5hmC-marked stalled replication forks by APE1 causes genomic instability. *Sci. Signal*, **13** , eaba8091.
36. Whitaker,A.M., Flynn,T.S. and Freudenthal,B.D. (2018) Molecular snapshots of APE1 proofreading mismatches and removing DNA damage. *Nat. Commun.*, **9**, 399.
37. Henricksen,L.A., Umbricht,C.B. and Wold,M.S. (1994) Recombinant replication protein A: expression, complex formation, and functional characterization. *J. Biol. Chem.*, **269**, 11121–11132.
38. Li,M., Sengupta,B., Benkovic,S.J., Lee,T.H. and Hedglin,M. (2020) PCNA monoubiquitination is regulated by diffusion of Rad6/Rad18 complexes along RPA filaments. *Biochemistry*., **59**, 4694–4702.
39. Yates,L.A., Aramayo,R.J., Pokhrel,N., Caldwell,C.C., Kaplan,J.A., Perera,R.L., Spies,M., Antony,E. and Zhang,X. (2018) A structural and dynamic model for the assembly of replication protein A on single-stranded DNA. *Nat. Commun.*, **9**, 5447.
40. Hormeno,S., Wilkinson,O.J., Aicart-Ramos,C., Kuppa,S., Antony,E., Dillingham,M.S. and Moreno-Herrero,F. (2022) Human HELB is a processive motor protein that catalyzes RPA clearance from single-stranded DNA. *Proc. Natl. Acad. Sci. U.S.A.*, **119**, e2112376119.
41. Maher,R.L. and Bloom,L.B. (2007) Pre-steady-state kinetic characterization of the AP endonuclease activity of human AP endonuclease 1. *J. Biol. Chem.*, **282**, 30577–30585.
42. He,H., Chen,Q. and Georgiadis,M.M. (2014) High-resolution crystal structures reveal plasticity in the metal binding site of apurinic/apyrimidinic endonuclease I. *Biochemistry*, **53**, 6520–6529.
43. Mol,C.D., Izumi,T., Mitra,S. and Tainer,J.A. (2000) DNA-bound structures and mutants reveal abasic DNA binding by APE1 and DNA repair coordination. *Nature*, **403**, 451–456.
44. Adams,P.D., Afonine,P.V., Bunkoczi,G., Chen,V.B., Davis,I.W., Echols,N., Headd,J.J., Hung,L.W., Kapral,G.J., Grosse-Kunstleve,R.W. *et al.* (2010) PHENIX: a comprehensive Python-based system for macromolecular structure solution. *Acta Crystallogr. D Biol. Crystallogr.*, **66**(Pt 2), 213–221.
45. Emsley,P. and Cowtan,K. (2004) Coot: model-building tools for molecular graphics. *Acta Crystallogr. D Biol. Crystallogr.*, **60**, 2126–2132.
46. Wang,Q.M., Yang,Y.T., Wang,Y.R., Gao,B., Xi,X.G. and Hou,X.M. (2019) Human replication protein A induces dynamic changes in single-stranded DNA and RNA structures. *J. Biol. Chem.*, **294**, 13915–13927.
47. Salas,T.R., Petruseva,I., Lavrik,O. and Saintome,C. (2009) Evidence for direct contact between the RPA3 subunit of the human replication protein A and single-stranded DNA. *Nucleic Acids Res.*, **37**, 38–46.
48. Kuppa,S., Deveryshetty,J., Chadda,R., Mattice,J.R., Pokhrel,N., Kaushik,V., Patterson,A., Dhingra,N., Pangeni,S., Sadauskas,M.K. *et al.* (2022) Rtt105 regulates RPA function by configurationally stapling the flexible domains. *Nat. Commun.*, **13**, 5152.
49. Freudenthal,B.D., Beard,W.A., Cuneo,M.J., Dyrkheeva,N.S. and Wilson,S.H. (2015) Capturing snapshots of APE1 processing DNA damage. *Nat. Struct. Mol. Biol.*, **22**, 924–931.
50. Fairlamb,M.S., Whitaker,A.M. and Freudenthal,B.D. (2018) Apurinic/apyrimidinic (AP) endonuclease 1 processing of AP sites with 5′ mismatches. *Acta Crystallogr. D Struct. Biol.*, **74**, 760–768.
51. Wold,M.S. (1997) Replication protein A: a heterotrimeric, single-stranded DNA-binding protein required for eukaryotic DNA metabolism. *Annu. Rev. Biochem.*, **66**, 61–92.
52. Li,J., Zhao,H., McMahon,A. and Yan,S. (2022) APE1 assembles biomolecular condensates to promote the ATR-Chk1 DNA damage response in nucleolus. *Nucleic Acids Res.*, **50**, 10503–10525.
53. Lin,Y., Li,J., Zhao,H., McMahon,A., McGhee,K. and Yan,S. (2022) APE1 recruits ATRIP to ssDNA in an RPA-dependent and-independent manner to promote the ATR DNA damage response. *Elife*.,**12**, e82324.
54. Nguyen,B., Sokoloski,J., Galletto,R., Elson,E.L., Wold,M.S. and Lohman,T.M. (2014) Diffusion of human replication protein A along single-stranded DNA. *J. Mol. Biol.*, **426**, 3246–3261.
55. Kim,C. and Wold,M.S. (1995) Recombinant human replication protein A binds to polynucleotides with low cooperativity. *Biochemistry*, **34**, 2058–2064.
56. Kim,C., Paulus,B.F. and Wold,M.S. (1994) Interactions of human replication protein A with oligonucleotides. *Biochemistry*, **33**, 14197–14206.
57. Blackwell,L.J. and Borowiec,J.A. (1994) Human replication protein A binds single-stranded DNA in two distinct complexes. *Mol. Cell Biol.*, **14**, 3993–4001.
58. Kolpashchikov,D.M., Khodyreva,S.N., Khlimankov,D.Y., Wold,M.S., Favre,A. and Lavrik,O.I. (2001) Polarity of human replication protein A binding to DNA. *Nucleic Acids Res.*, **29**, 373–379.

59. Wilson,D.M. 3rd (2005) Ape1 abasic endonuclease activity is regulated by magnesium and potassium concentrations and is robust on alternative DNA structures. *J. Mol. Biol.*, **345**, 1003–1014.
60. Berquist,B.R., McNeill,D.R. and Wilson,D.M. 3rd (2008) Characterization of abasic endonuclease activity of human Ape1 on alternative substrates, as well as effects of ATP and sequence context on AP site incision. *J. Mol. Biol.*, **379**, 17–27.
61. Li,M. and Wilson,D.M. 3rd (2014) Human apurinic/apyrimidinic endonuclease 1. *Antioxid. Redox Signal.*, **20**, 678–707.
62. Schermerhorn,K.M. and Delaney,S. (2014) A chemical and kinetic perspective on base excision repair of DNA. *Acc. Chem. Res.*, **47**, 1238–1246.
63. Tumbale,P., Williams,J.S., Schellenberg,M.J., Kunkel,T.A. and Williams,R.S. (2014) Aprataxin resolves adenylated RNA-DNA junctions to maintain genome integrity. *Nature*, **506**, 111–115.
64. Comeaux,E.Q., Cuya,S.M., Kojima,K., Jafari,N., Wanzeck,K.C., Mobley,J.A., Bjornsti,M.A. and van Waardenburg,R.C. (2015) Tyrosyl-DNA phosphodiesterase I catalytic mutants reveal an alternative nucleophile that can catalyze substrate cleavage. *J. Biol. Chem.*, **290**, 6203–6214.
65. Burkovics,P., Hajdu,I., Szukacsov,V., Unk,I. and Haracska,L. (2009) Role of PCNA-dependent stimulation of 3′-phosphodiesterase and 3′-5′ exonuclease activities of human Ape2 in repair of oxidative DNA damage. *Nucleic Acids Res.*, **37**, 4247–4255.
66. Wiederhold,L., Leppard,J.B., Kedar,P., Karimi-Busheri,F., Rasouli-Nia,A., Weinfeld,M., Tomkinson,A.E., Izumi,T., Prasad,R., Wilson,S.H. *et al.* (2004) AP endonuclease-independent DNA base excision repair in human cells. *Mol. Cell*, **15**, 209–220.
67. Kuznetsova,A.A., Matveeva,A.G., Milov,A.D., Vorobjev,Y.N., Dzuba,S.A., Fedorova,O.S. and Kuznetsov,N.A. (2018) Substrate specificity of human apurinic/apyrimidinic endonuclease APE1 in the nucleotide incision repair pathway. *Nucleic Acids Res.*, **46**, 11454–11465.
68. Burra,S., Marasco,D., Malfatti,M.C., Antoniali,G., Virgilio,A., Esposito,V., Demple,B., Galeone,A. and Tell,G. (2019) Human AP-endonuclease (Ape1) activity on telomeric G4 structures is modulated by acetylatable lysine residues in the N-terminal sequence. *DNA Repair (Amst.)*, **73**, 129–143.
69. Alekseeva,I.V., Kuznetsova,A.A., Bakman,A.S., Fedorova,O.S. and Kuznetsov,N.A. (2020) The role of active-site amino acid residues in the cleavage of DNA and RNA substrates by human apurinic/apyrimidinic endonuclease APE1. *Biochim. Biophys. Acta Gen. Subj.*, **1864**, 129718.
70. Kim,W.C., Berquist,B.R., Chohan,M., Uy,C., Wilson,D.M. 3rd and Lee,C.H. (2011) Characterization of the endoribonuclease active site of human apurinic/apyrimidinic endonuclease 1. *J. Mol. Biol.*, **411**, 960–971.
71. Hoitsma,N.M., Click,T.H., Agarwal,P.K. and Freudenthal,B.D. (2021) Altered APE1 activity on abasic ribonucleotides is mediated by changes in the nucleoside sugar pucker. *Comput. Struct. Biotechnol. J.*, **19**, 3293–3302.
72. Chou,K.M. and Cheng,Y.C. (2002) An exonucleolytic activity of human apurinic/apyrimidinic endonuclease on 3′ mispaired DNA. *Nature*, **415**, 655–659.
73. Hoitsma,N.M., Whitaker,A.M., Beckwitt,E.C., Jang,S., Agarwal,P.K., Van Houten,B. and Freudenthal,B.D. (2020) AP-endonuclease 1 sculpts DNA through an anchoring tyrosine residue on the DNA intercalating loop. *Nucleic Acids Res.*, **48**, 7345–7355.
74. Tsutakawa,S.E., Lafrance-Vanasse,J. and Tainer,J.A. (2014) The cutting edges in DNA repair, licensing, and fidelity: DNA and RNA repair nucleases sculpt DNA to measure twice, cut once. *DNA Repair (Amst.)*, **19**, 95–107.
75. Harrington,J.J. and Lieber,M.R. (1994) Functional domains within FEN-1 and RAD2 define a family of structure-specific endonucleases: implications for nucleotide excision repair. *Genes Dev.*, **8**, 1344–1355.
76. Harrington,J.J. and Lieber,M.R. (1995) DNA structural elements required for FEN-1 binding. *J. Biol. Chem.*, **270**, 4503–4508.
77. Huffman,J.L., Sundheim,O. and Tainer,J.A. (2005) DNA base damage recognition and removal: new twists and grooves. *Mutat. Res.*, **577**, 55–76.
78. Bennett,R.J., Dunderdale,H.J. and West,S.C. (1993) Resolution of Holliday junctions by RuvC resolvase: cleavage specificity and DNA distortion. *Cell*, **74**, 1021–1031.
79. Yang,W. (2011) Nucleases: diversity of structure, function and mechanism. *Q. Rev. Biophys*, **44**, 1–93.
80. Peddi,S.R., Chattopadhyay,R., Naidu,C.V. and Izumi,T. (2006) The human apurinic/apyrimidinic endonuclease-1 suppresses activation of poly(adp-ribose) polymerase-1 induced by DNA single strand breaks. *Toxicology*, **224**, 44–55.
81. Liu,T.C., Lin,C.T., Chang,K.C., Guo,K.W., Wang,S., Chu,J.W. and Hsiao,Y.Y. (2021) APE1 distinguishes DNA substrates in exonucleolytic cleavage by induced space-filling. *Nat. Commun.*, **12**, 601.
82. Izumi,T., Schein,C.H., Oezguen,N., Feng,Y. and Braun,W. (2004) Effects of backbone contacts 3′ to the abasic site on the cleavage and the product binding by human apurinic/apyrimidinic endonuclease (APE1). *Biochemistry*, **43**, 684–689.
83. Whitaker,A.M., Stark,W.J. and Freudenthal,B.D. (2022) Processing oxidatively damaged bases at DNA strand breaks by APE1. *Nucleic Acids Res.*, **50**, 9521–9533.
84. Adasme,M.F., Linnemann,K.L., Bolz,S.N., Kaiser,F., Salentin,S., Haupt,V.J. and Schroeder,M. (2021) PLIP 2021: expanding the scope of the protein-ligand interaction profiler to DNA and RNA. *Nucleic Acids Res.*, **49**, W530–W534.
85. Alcasabas,A.A., Osborn,A.J., Bachant,J., Hu,F., Werler,P.J., Bousset,K., Furuya,K., Diffley,J.F., Carr,A.M. and Elledge,S.J. (2001) Mrc1 transduces signals of DNA replication stress to activate Rad53. *Nat. Cell Biol.*, **3**, 958–965.
86. Kanoh,Y., Tamai,K. and Shirahige,K. (2006) Different requirements for the association of ATR-ATRIP and 9-1-1 to the stalled replication forks. *Gene*, **377**, 88–95.
87. MacDougall,C.A., Byun,T.S., Van,C., Yee,M.C. and Cimprich,K.A. (2007) The structural determinants of checkpoint activation. *Genes Dev.*, **21**, 898–903.
88. Chen,R. and Wold,M.S. (2014) Replication protein A: single-stranded DNA's first responder: dynamic DNA-interactions allow replication protein A to direct single-strand DNA intermediates into different pathways for synthesis or repair. *Bioessays*, **36**, 1156–1161.
89. Gibb,B., Ye,L.F., Gergoudis,S.C., Kwon,Y., Niu,H., Sung,P. and Greene,E.C. (2014) Concentration-dependent exchange of replication protein A on single-stranded DNA revealed by single-molecule imaging. *PLoS One*, **9**, e87922.
90. Chen,R., Subramanyam,S., Elcock,A.H., Spies,M. and Wold,M.S. (2016) Dynamic binding of replication protein a is required for DNA repair. *Nucleic Acids Res.*, **44**, 5758–5772.
91. Pokhrel,N., Caldwell,C.C., Corless,E.I., Tillison,E.A., Tibbs,J., Jocic,N., Tabei,S.M.A., Wold,M.S., Spies,M. and Antony,E. (2019) Dynamics and selective remodeling of the DNA-binding domains of RPA. *Nat. Struct. Mol. Biol.*, **26**, 129–136.